Excess Entropy Scaling in Supercooled Ternary Metallic Mixtures

Áron Kuna, Su Mei Gwen Ho, Andrea G. Martínez

A Subject Module Project in Physics

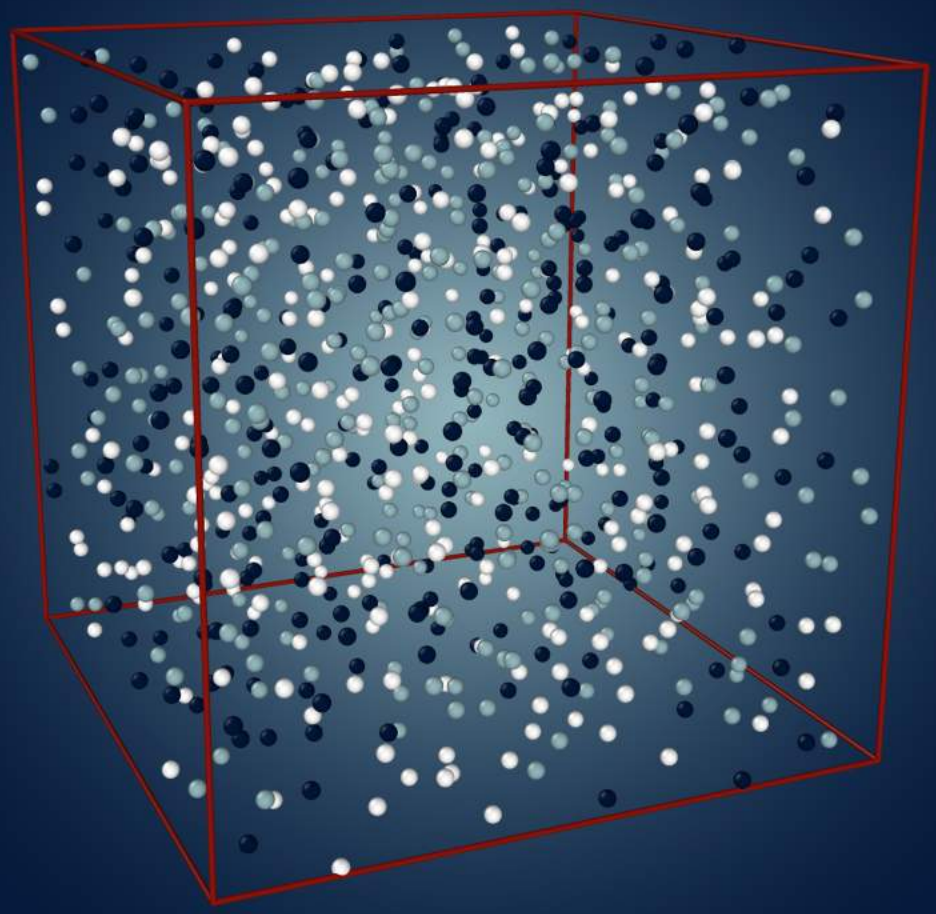

Supervisor: Trond Ingebrigtsen
Roskilde University
December 20, 2022

Abstract

This report investigates how excess entropy scaling affects transport coefficients for ternary (three-component) supercooled mixtures, building upon previous studies which have been conducted for large systems of supercooled single-component and binary mixtures. The results indicate quasi-universal excess entropy scaling across different temperatures for a given mixture, a collapse which continues to hold across the two compositions of the KA mixture, KA 8:2:2 and KA 8:2:4; as well as across two different models, the KA model and the WS model. This quasi-universality appears to operate in a similar, but not equivalent manner to the correlation found for binary mixtures in a previous study [6]. More research is required to delve into how excess entropy scaling works, and how multi-component supercooled systems can take advantage of this functionality.

Contents

1 Introduction

Any liquid can be cooled down fast enough so that it enters a supercooled state [18]. Supercooled liquids approaching the glass transition can display a particular phenomenon; a slight change in temperature or density significantly affects transport coefficients such as viscosity and diffusion coefficient [6]. Although this phenomenon has been extensively studied, the driving mechanism behind it remains unknown. One theory proposed in 1977 by Yaakov Rosenfeld is that transport coefficients of supercooled liquids are some function of excess entropy, the leftover entropy when entropy of an ideal gas is removed from the total entropy of a system [21]. This quasi-universal theory has been studied for several decades now, through molecular dynamic (MD) computer simulations. In 2020 Bell, Dyre and Ingebrigtsen published an extensive study demonstrating quasi-universal, almost composition-independent excess entropy scaling for a range of binary mixtures [6]. As a natural progression, this report aims to investigate if this relationship continues to hold for supercooled ternary (three-component) mixtures.

In this report, three supercooled ternary mixtures are examined using MD simulations, run on high-performance Nvidia Geforce GTX 1080 graphics cards at Roskilde University (RUC) using the Roskilde University Molecular Dynamics (RUMD) package, version 3.6. First a 12000 particle Kob-Andersen (KA) model is studied, where the ratio of the types of particles is 8:2:2. Then the composition of the model is then changed to 8:2:4. Finally, a 900 particle Wahnström (WS) model is studied, where the ratio of particle types is equal parts (1:1:1). These experiments followed a steep learning curve, due to time constraints and a lack of experience with MD simulations. The process was iterative and closely supervised by Professor Trond Ingebrigtsen.

The report contains some background theory on relevant thermodynamic concepts, a basic explanation of how MD simulations work, and how RUMD is utilised; the results and discussion follow.

1.1 Research Question

The research question is formulated as such:

How does excess entropy control transport properties in supercooled ternary mixtures?

The following sub-questions are designed to guide the report:

1. To what extent does excess entropy scaling hold for various densities and temperatures?
2. To what extent is there quasi-universality as a function of composition?
3. To what extent is there quasi-universality between ternary mixtures?
4. To what extent does quasi-universality hold amongst binary and ternary mixtures?

2 Theory

2.1 Thermodynamics

Symbol	Name
T	temperature
N	number of particles
V	volume
ρ	density
S	entropy of the system
S_{ex}	excess entropy
S_{id}	entropy of an ideal gas
A	Helmholtz free energy
A_{ex}	excess free energy
A_{id}	free energy of an ideal gas
E	total energy of a system
D	diffusion coefficient
W	virial
U	potential energy

Table 1: Symbols needed for the following section.

2.1.1 Supercooled Liquids

Thermodynamics dictates that a material should obtain a lower free energy state by attaining a crystalline structure as it is cooled from a liquid, a process known as crystallisation. However, it is possible to cool a liquid below its freezing temperature and avoid crystallisation; this is called supercooling. A supercooled liquid is thermodynamically unstable yet may remain in this state for an extended period of time [13,18]. When cooled further, the liquid falls out of equilibrium and vitrifies; entering a glass transition. The glass transition is a gradual change from a viscous liquid to a "glass" state which is not crystalline in nature. The temperature at which a glass is formed, is referred to as the glass transition temperature, T_g [8]. Although the glass transition is an exciting area of research in physics, chemistry and material sciences, it is not the focus of this report.

It has been observed that most liquids approaching the glass transition display dramatic changes in transport properties such as viscosity with only slight changes in temperature or density [18]. The "Angell plot" published in 1989, see Figure 1, summarises this phenomenon. Here, the logarithm of viscosity μ of a system is plotted against T_g over temperature T. During the cooling process, some liquids show Arrhenius behaviour (displayed as straight lines) while others show non-Arrhenius behaviour (exponential curves), for the purposes of this project, this is not the main focus. Until today, a universally-accepted theory which explains the large changes in the transport coefficients of supercooled liquids is yet to be established [7].

2.1.2 Excess Entropy Scaling

Two transport properties of note when it comes to supercooled liquids are viscosity and diffusivity. Due to time constraints, this project will focus solely on the diffusion coefficient D.

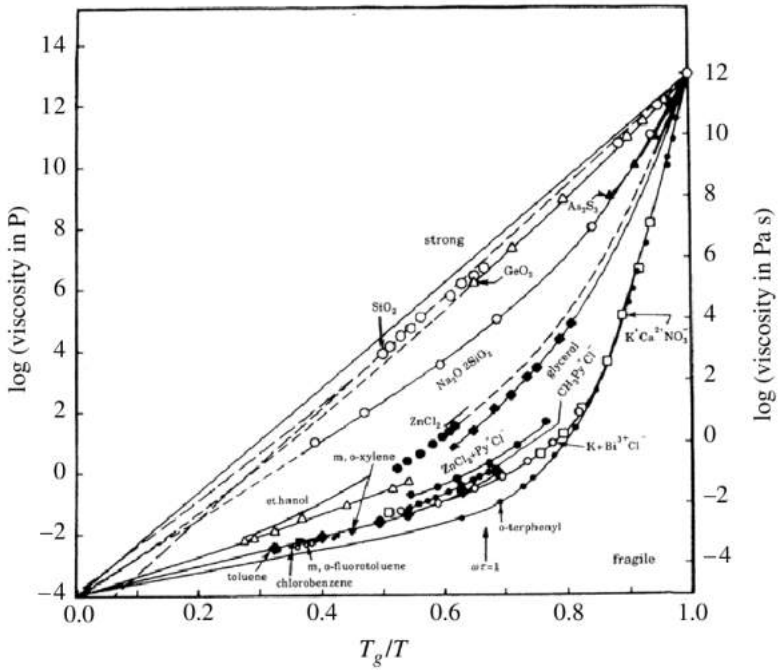

Figure 1: Angell's plot showing Arrhenius and non-Arrhenius increases in the viscosity of various systems as they approach the glass transition [7].

Consider a system with constant temperature T and density $\rho \equiv N/V$, where N is the number of particles and V is the volume. The system's entropy S is a function of both temperature and density. The excess entropy of the system S_{ex} can then be defined as what remains when the entropy of an ideal gas S_{id} at the temperature and density is subtracted from the total entropy:

$$S_{ex}(\rho, T) \equiv S(\rho, T) - S_{id}(\rho, T) \tag{1}$$

In 1977, Yaakov Rosenfeld published a paper "Relation between the transport coefficients and the internal entropy of simple systems" [21]; in it he proposed a quasi-universal theory, that some transport property X in reduced units could be expressed as some function of excess entropy:

$$\tilde{X} = f(S_{ex})\,[11] \tag{2}$$

Since then, there have been numerous attempts to explain "excess entropy scaling".

The "reduced units" employed by excess entropy scaling vary according to the temperature and density of the system, in other words, the thermodynamic state point. These dimensionless units can be made by measuring length, energy and mass in terms of macroscopic properties. For example, D which is defined as length squared over time, $D = l^2/t$, is defined in reduced units as:

$$\tilde{D} \equiv (\rho^{1/3}\sqrt{m/k_B T})D\,[11] \tag{3}$$

where the tilde is used to denote a reduced unit, m is particle mass and k_B is Boltzmann's constant.

2.1.3 Calculating Excess Entropy

Entropy describes the disorder of a system or loosely speaking, the randomness. The molecules in an ideal gas are equally distributed over its volume reaching the maximum possible randomness for

the given macroscopic thermodynamic condition, resulting in the maximum entropy for this macro state. Repeating this equation 1, excess entropy is defined as:

$$S_{ex}(\rho, T) \equiv S(\rho, T) - S_{id}(\rho, T) \tag{4}$$

Excess entropy gives a measure of the order in the system compared to the maximum possible disorder. Since $S(\rho, T) \leq S_{id}(\rho, T)$, the excess entropy is either zero or a negative quantity.

The excess entropy of a system is not given by the simulations in RUMD however, it can be calculated. To calculate the excess entropy, the Helmholtz free energy equation can be used which is defined as:

$$A = E - TS \tag{5}$$

which in statistical mechanics can be written as.

$$A_{ex} = U_{ex} - TS_{ex} \tag{6}$$

The potential energy U_{ex} is calculated in the simulation (by summing up the potentials of all the particles). Then to get the excess entropy the excess free energy need to be calculated.

$$TS_{ex} = U_{ex} - A_{ex} \tag{7}$$

To get the excess free energy the strategy is to start at a reasonably high temperature and low density. This is the starting point where due to the low density the particles barely interact with each other which makes the characteristics of the substance approach an ideal gas. It means that the excess free energy (A_{ex}) is close to zero. (Since $A_{ex} = A - A_{id}$ where A is the free energy of the system and it approximately equals A_id). Then integrate the virial over density to reach the desired density point. Finally integrate the potential energy over temperature while the density is constant to get the free energy values for lower temperatures. The process is further explained below.

Constant Temperature

The excess free energy is calculated from the virial. For constant temperature and fixed number of particles the virial is defined as:

$$W = (\frac{\partial A_{ex}}{\partial \ln \rho})_{N,T} \tag{8}$$

which can be reformulated as (N and T are still constants)

$$\int_{A_{ex,0}}^{A_{ex,1}} dA_{ex} = \int_{\rho_0}^{\rho_1} W(\rho)\, d\ln\rho \tag{9}$$

$$A_{ex,1} - A_{ex,0} = A_{ex,1} = \int_{\rho_0}^{\rho_1} W(\rho)\, d\ln\rho \tag{10}$$

$A_{ex,0} \approx 0$ as explained above. To get the virial function with respect to density in the equation, the virial is calculated in simulations for several densities at constant temperature then a function can be fit with good approximations. The virial is calculated from the position of the particles and the forces acting on them [4]. Both of them are known in a simulation.

$$W = \frac{1}{3} \sum_i \sum_{j>i} r_{ij} \cdot f_{ij} \tag{11}$$

Where $\sum_i \sum_{j>i} r_{ij}$ denotes the sum of particle pairs, counted once for each pair.

Constant density

Calculating the excess entropy when the density is kept constant is a similar process to constant temperature. However, instead of equation 8 the free energy is calculated from the potential energy.

$$U_{ex} = (\frac{\partial(\beta A_{ex})}{\partial\beta})_{N,V} \tag{12}$$

From which the free energy equals:

$$\int_{A_{ex,1}}^{A_{ex,2}} d\beta A_{ex} = \int_{\beta_0}^{\beta_1} U_{ex}(\beta)\, d\beta \tag{13}$$

Where β is $\frac{1}{kT}$. Much as the virial, the potential energy is calculated for several temperatures. Which is used to fit a function of potential energy with respect to temperature (β). Since $A_{ex,1}$ is known, inserting the function in the equation above gives a simple integration to get $A_{ex,2}$.

$$A_{ex,2} = \int_{\beta_0}^{\beta_1} U_{ex(\beta)}\, d\beta + A_{ex,1} \tag{14}$$

Finally $A_{ex,2}$ is inserted into equation 7. Subtracting $A_{ex,2}$ from the potential energy gives the excess entropy.

With this method, the excess entropy values are calculated for a specified temperature range at a specified density. How the method is implemented in practice is explained in chapter 3.4

2.1.4 Roskilde Simple Liquids

In 2006, a new class of liquids, Roskilde Simple (RS) liquids, were discovered. The research on RS liquids and their properties is extensive, however only the basic concepts required for the scope of this report will be covered. RS liquids are defined by a high correlation coefficient $R \geq 0.9$, where R describes the relationship between fluctuations in the potential energy U and the microscopic virial W in a system in equilibrium:

$$R = <\Delta W \Delta U> / \sqrt{<(\Delta U)^2><(\Delta W)^2>}\,[11] \tag{15}$$

where W is the excess pressure in the system, defined as $W = PV - NkBT$ [10], and the angular brackets indicate an NVT ensemble average.

In addition, an RS liquid has "isomorphs" to a good approximation [18]. Isomorphs are curves found in the system's thermodynamic phase diagram, for which properties such as excess entropy and the diffusion coefficient are invariant in reduced units. Given that these properties are invariant along the same curves, isomorphs show that Rosenfeld scaling (Eq. (15) holds [6].

RS liquids have been observed in both experimental settings and in MD simulations, and include most if not all van der Waals and metallic liquids; however covalent-bonding and ionic liquids are excluded [6]. Model systems which have been studied and classified as RS liquids include the standard single-component Lennard Jones (LJ) liquid, the Kob-Andersen binary LJ (KA) mixture and the Wahnström binary LJ (WS) mixture amongst others [18]. These models will be elaborated upon in the Section 2.2.

2.1.5 Current Research

This section will give an brief overview of research which has been conducted on excess entropy scaling. Since Rosenfeld's discovery, excess-entropy scaling has been the subject of a broad range of studies, both simulation and experimental, investigating atomic mixtures, molecular liquids, confined systems, etc [6]. In particular, simulations have provided much evidence for excess entropy scaling. An extensive review of excess entropy scaling reports can be found in ref. [11]. To date, excess entropy has been found to apply more generally than initially anticipated; however, it cannot be thought of

as a general theory, as it has exceptions [11]. An exception of note is that the quasi-universal excess entropy scaling does not hold for molecules in general [6], such as the standard water model [11].

Excess entropy scaling has been shown to be relevant to industrial applications; models based on excess entropy scaling have been found to provide a functional way of determining transport coefficients in engineering settings. Applications include methane and hydrogen absorption in metal-organic frameworks, the viscosity and thermal conductivity of refrigerants, transport properties of electrolytes and silica melts.

A subject of interest for this report is how excess entropy scaling holds for mixtures of atoms, as they are commonly used in simulations and experiments in order to prevent crystallisation as well as enhance desirable properties. This is an especially intriguing area as mixtures such as metallic alloys may have atoms of different masses, varying compositions, and interactions between particles may differ. Therefore, quasi-universality is not expected. Excess entropy scaling in binary mixtures has been studied with varying success; a poor relationship has been found for binary hard sphere mixtures, tetrahedral-forming ionic melt and other simple mixtures have not demonstrated a universal collapse, however LJ mixtures in the high-temperature regime over a limited range in viscosity have shown universality [6].

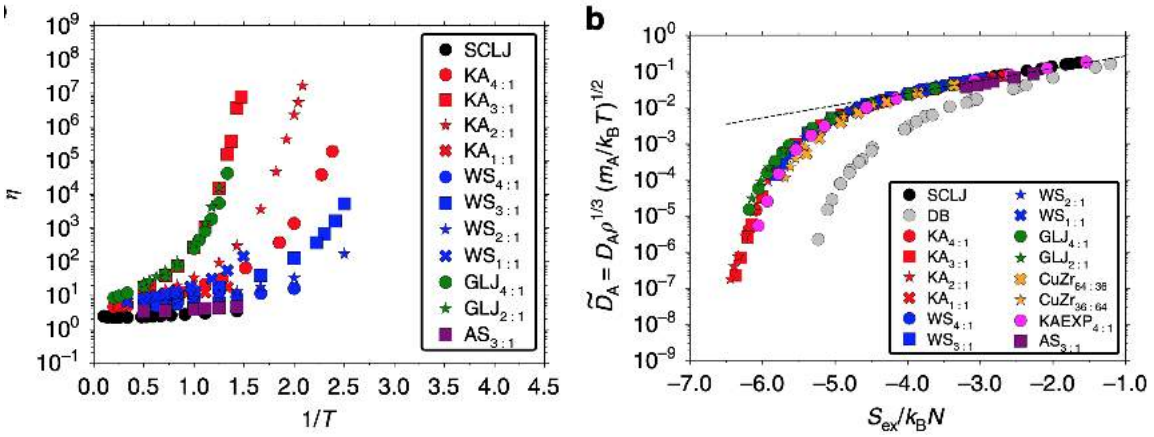

(a) (b)

Figure 2: (a) A plot showing the non-Arrhenius correlation between viscosity and temperature, for various supercooled binary metallic mixtures and one single-component metallic model (SCLJ) [6]. (b) A plot showing a quasi-universal collapse in the correlation between the reduced diffusion coefficient and excess entropy, for various supercooled binary mixtures and compositions. A dumbbell molecule (DB) and SCLJ are shown as a reference point [6].

A recent simulation study of note investigated excess entropy scaling for several binary mixtures and compositions, finding a composition-independent relationship between transport coefficients and excess entropy, see Figure 2a. In addition, a quasi-universal collapse was found amongst different mixtures, see Figure 2b. Some deviations are seen for most supercooled states, hence the term quasi-universal. The question remains, does excess entropy control transport coefficients, or vice versa? The six binary mixtures studied are the KA mixture, the WS mixture and well as the generalised LJ (GLJ) mixture, the KA exponential pair potential (KAEXP) mixture, alloys of copper and zirconium (CuZr), and a size asymmetric (AS) mixture. A similar study for three-component mixtures has yet to be conducted; such an investigation would be especially interesting as it is thought that excess entropy scaling could facilitate the design of future metallic alloys [6].

2.2 Molecular Dynamics

Molecular dynamics is a tool to find the properties of molecular systems. Due to the large number of particles in such systems, the properties cannot be determined analytically [4]. Molecular dynamics is a solution where the positions of the atoms and molecules are known, and for small time steps, the new positions are numerically calculated. The new positions are calculated by solving Newton's equations of motion for each particle. The well-known second law of Newton is expressed as follows:

$$F = ma \tag{16}$$

F is the force, a the acceleration, and the mass is given by m. Furthermore, in the case of the free fall of a body, which means that it is only affected by gravity, the second law is written as:

$$mg = m\frac{d^2y}{dt^2} \tag{17}$$

where g is the gravitational acceleration. A coordinate system is applied with the $y-axis$ which is in the direction of the force on the body [18]. Solving for y, the result is a second-order ordinary differential equation. It is one of the main and most known results is classical mechanics:

$$y = \frac{1}{2}gt^2 + v_{0_y}t + y_0 \tag{18}$$

v_{0_y} and y_0 are the initial conditions, known as integration constants. The previous equation is set to determine the motion of the particle in the past, present, and future when the only force acting is the gravitational force. [18].

Solving Newton's equations for a molecular system increases the complexity significantly. For a system of N particles, each particle has an effect on every other particle. This effect can be represented as a potential energy function. Then the force is given by $F = -\nabla U(r_1...r_N)$. ∇ is the gradient operator and r_k denotes the position vector of particle k. [18]. The potential function U is the sum of potentials between particle pairs.

$$U = \sum_{i<j} v(r_{ij}) \tag{19}$$

r_{ij} represents the distance between the particle pairs.

Solving Eq. 19 is not possible analytically due to the large number of particles in molecular systems, as mentioned above. The way to solve it is through using a numerical integrator, for example, the leap-frog algorithm which is further explained in Section 2.2.2. There are several advantages to molecular dynamics. The positions and velocities are known for each particle which allows observations that are complicated or impossible in real-life experiments. The biggest disadvantage of the method is the required computational power since the calculations have to be made for every time step. The required time steps can be enormous as for example, when the simulation involves femtosecond vibrations.

2.2.1 Interaction Between Molecules

As mentioned, in a simulation the potential energy is separated into potential energy between particle pairs. These can be summed up to get an accurate approximation for the potential energy of the macroscopic thermodynamic system when there is no external force. To get a more precise macroscopic potential energy, not just the pair potentials but the triplets should be calculated as well. The computational power to calculate the potential energy for triplets is so immense that

it is usually neglected or included in the pair potential. The pair potential including the three-body effects is called the effective pair potential. Of course, it gives an approximation, not precise results. [4]

Specifying the potential between particles allows for modelling systems without setting sub-nuclear details. The potential describes how the particles interact with each other. Therefore once the potentials are known a system can be modelled by knowing the positions and momenta of the particles and then calculating the Newtonian mechanics for small time steps. The force on a particle is given by summing up the effects of the potentials of all the other particles in the system. However to lower the number of required calculations a limit can be set for the distance for which the potentials are calculated.

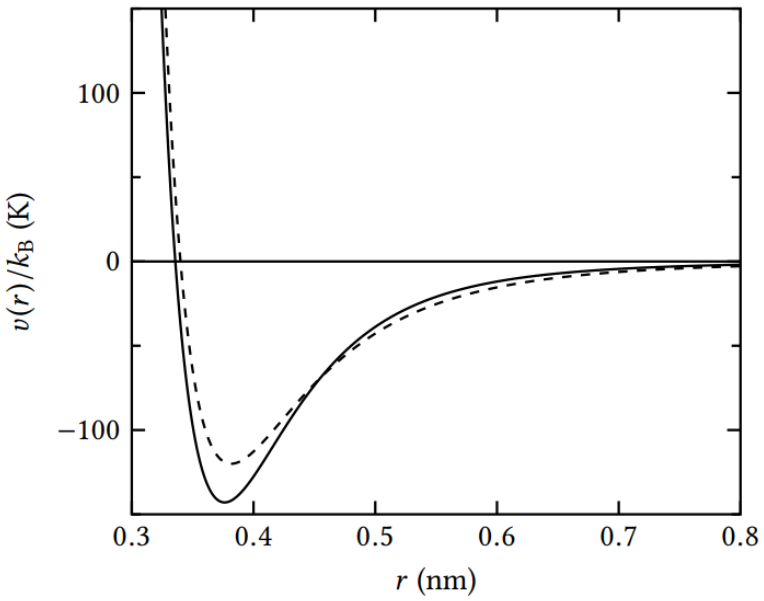

Figure 3: The potential of liquid Argon particle pairs as a function of separation (continuous line). It is approximated by the Lennard-Jones 12-6 potential (dashed line) which is used in MD simulations. The x-axis is the distance between the particle pair. The y-axis is the potential energy (Source: *Computer Simulation of Liquids page 7*[4]).

The pair potential depends on the type of atom or molecule. In a two-component system where there is particle type A and B, the potential is different between particle A to A to A to B. Therefore in a simulation the potential has to be set for each type and between the separate types. This results in 3 different potentials for a two-component mixture since A to B is the same as B to A. For three-component, the number of required potentials is six. (Generally, the number of potentials is $\binom{2}{n} + n$ where n is the number of particle types.)

The pair potential is a function of potential energy over the distance separating the particle pair, see Figure 3. Generally, when the distance is relatively small (the atoms are close to each other) the potential energy is high and gets lower with separation. After some distance, the potential energy reaches its minimum and starts to grow again. At the subatomic level this change is due to the positioning of the electrons but as mentioned above, using the potentials gives a good approximation for these inner mechanics. [4]

To lower the computer power the goal is to have simple potentials, however, detailed enough to give usable results. A commonly used potential is the Lennard-Jones pair potential U^{LJ}. With properly set parameters ($\epsilon/k_B = 120K, \sigma = 0.34nm$) it approximates the pair potential of liquid argon atoms.

$$U^{LJ}(r) = 4\epsilon[(\sigma/r)^{12} - (\sigma/r)^6] \tag{20}$$

In the equation, σ is the distance where the potential energy is zero. ϵ is the minimum value of the potential energy in other words the "depth of the well" [4]. The force acting on the particles is

$$F = -\frac{dU}{dr} \tag{21}$$

Positive force means repulsive and negative force means attractive interaction between the particle pair. Changing the σ and ϵ values in the LJ potential gives potentials that can be used to simulate different substances. Two potentials that are used in the report are detailed below.

Kob-Andersen

The KA model was made with the aim to describe the glass transition in the structural glasses. It is a binary mixture of the LJ pairs, designed to describe the physical properties of simple metallic gasses. However, this model has served as a standard in computer modelling for long simulations of high-viscosity liquids [22]. The parameters for KA are: $\sigma_{AA} = 1$, $\sigma_{BB} = 0.88$,$\sigma_{AB} = 0.80$ and $\epsilon_{AA} = 1$, $\epsilon_{BB} = 0.50$, $\epsilon_{AB} = 1.50$, in this case the mass is the same for both particles [6]. The KA potential creates a strong non-ideal mixture, due to the fact that an AB attraction is three times stronger than a BB attraction. [22]

Wahnström

Similar to the KA model, the WS model does not crystallise easily. Originally proposed by Wahnström for the study of viscous liquid dynamics [23], this model uses the LJ 12-6 potential as well. The parameters are $\sigma_{AA} = 1.2$, $\sigma_{BB} = 1.0$, $\sigma_{AB} = 1.1$ and $\epsilon_{AA} = \epsilon_{BB} = \epsilon_{AB} = 1$; dissimilar to the KA model, $m_a = 2.0$ and $m_B = 1.0$ [6].

2.2.2 Integrator

As mentioned in Section 2.2, a numerical integrator is needed to calculate Newton's laws for each particle. A commonly used way is the Leap-frog algorithm, which is the one used in this project. Is a method for solving ordinary differential equations (ODE), see the example below:

$$x'' = \frac{d^2x}{dt^2} = H(x) \tag{22}$$

in this simple case, x is a function of t, where t represents time and x the position.

The leapfrog algorithm solves the second-order ODE in a direct way. It is important to emphasize that ODE solvers work with first-order equations. This means that to be able to solve a second-order equation, the second-order ODE must be turned into a system of first-order equations by introducing the first derivative of the solution as a new variable [1]. The second thing that differentiates this method from others is that it is reversible, which means, when time is reversed, it can step back to exactly where it began, apart from any loss of accuracy due to floating point. An important and useful property of the leapfrog integrator is that it conserves energy. It can perform a lot better over a long period of time in comparison to other methods that may be more accurate for short simulations. [1]

In leapfrog, the next equations are for updating the position and the velocity:

$$h_i = H(x_i), \tag{23}$$

$$v_{i+1/2} = v_{i-1/2} + h_i\Delta t, \tag{24}$$

$$x_{i+1} = x_i + v_{i+1/2}\Delta t, \tag{25}$$

x_i is the position at step i, $v_{i+1/2}$ is the velocity, also known as the first derivative of x. h_i is the second derivative of x or acceleration at step i and Δt step. All these equations are expressed in a way that gives the velocity at integer steps as follows:

$$x_{i+1} = x_i + v_i\Delta t + \frac{1}{2}h_i\Delta t^2, \tag{26}$$

$$v_{i+1} = v_i + \frac{1}{2}(h_i + h_{i+1})\Delta t \tag{27}$$

2.2.3 Periodic Boundary

The investigation of a thermodynamic system through simulation often means monitoring the effect of the inter-molecular forces on the macroscopic characteristics. To get good statistics the effects of external forces on the system should be minimised. It raises the question of how to keep the density fixed.

The obvious solution is to set boundaries which can be achieved by setting some external potentials acting on the particles in the shell. However, the effects of these outside potentials are significant. The common number of particles for molecular dynamics simulations range from 10 to 10000 [4]. In a system of 8000 particles simulated in a cube, $19^3 = 6859$ particles are inside leaving 1141 particles to be affected by the boundary potentials. That is more than 14% of the particles. (For a sphere it is 4% which is still significant and using a sphere complicates the simulation in other ways). Even if the simulated substance is kept together by cohesive forces the particles on the surface will experience significantly different forces than the interior particles.

The ideal simulation would be where an infinitely large body is simulated where there is no boundary at all while the particle number is as low as possible. Using periodic boundary conditions [4] offers a close enough system to this ideal. The solution is to repeat the simulated box in all directions then repeat those copies of the original box again and so on creating an infinite lattice based on the "centre" box. The positions of the particles are exactly copied. Then when a particle, for example, leaves the box at the bottom another comes into its place at the top. It acts as if it was infinite however, it is enough to keep account of the particles in the original box for the simulation. This way there are no boundary effects on the particles.

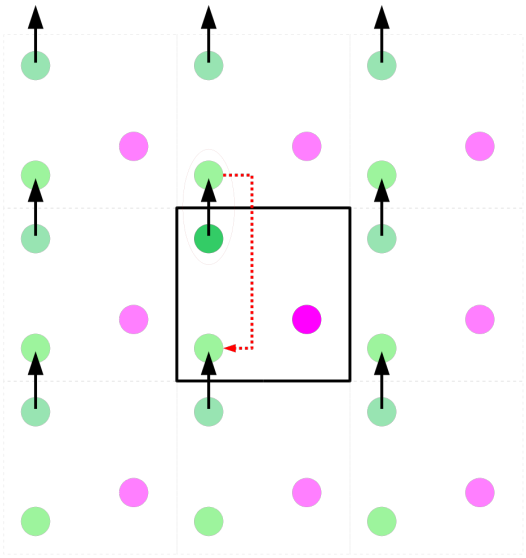

Figure 4: Periodic boundary conditions represented in 2D. The same concept is applied in three dimensions in a lattice of infinitely repeating boxes [16].

Figure 4 shows the concept in two dimensions. For two dimensions the system can be imagined as a torus map where a particle always going in the same direction will just circle around the "doughnut".

The obvious problem that rises with this solution is that the particles can interact with themselves or one particle interacts with several images of another particle. However, a quick fix for this is to set the cutoff for the potentials to be less than half of the length of the box [4]. This way any particle will interact, at the most, once with any other particle during one time step.

2.2.4 Post-Processing

The following section briefly explains three analytical tools used to process simulation results. The radial distribution function (RDF) is used to understand the structure of the system, the intermediate scattering function (ISF) is for looking at the time dependant correlations which provides information abut the behaviour of liquids upon supercooling, and the mean squared distribution measures the displacement of a particle from its origin.

Radial Distribution Function

The RDF in simple terms relates to the probability of finding a particle at some distance r from another particle. When a system is in a fluid phase, the liquid or gas is homogeneous and isotropic. The number of particles in the spherical "shell" of a given particle, at distance r, is given by:

$$dN_{ID} = 4\pi\rho r^2 dr \tag{28}$$

for N particles randomly distributed in a volume in an ideal gas [13]. See Figure 5.

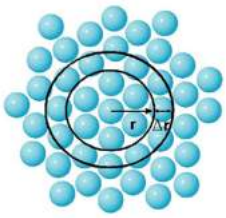

Figure 5: A figure showing the radial distribution of particles in some lattice, at distance r from the origin [13].

In order to account for interaction between particles, Eq. 28 is adjusted to to describe how the distribution of the particles locally deviates from the uniform distribution of an ideal gas, where $g(r) = 1$.

$$dN = 4\pi\rho g(r) r^2 dr \text{ [13]} \tag{29}$$

The g(r) is a normalised distribution function that can be obtained from experiments. It can also be derived using statistical mechanics, which is not within the scope of this report. As r increases, particle interaction decays to zero and $g(r)$ typically approaches 1. For state points in a system in the liquid phase, the RDF will show several well-defined peaks; the first peak corresponds to the closest shell, the "nearest-neighbour" shell, the second peak corresponds to the second closest shell of neighbours, etc [13]. Figure 6 shows how the peaks of the RDF plot relate to the shells of neighbours.

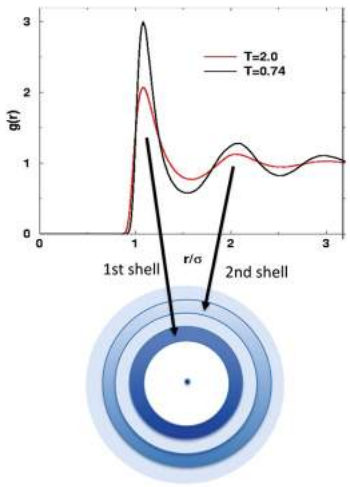

Figure 6: A plot showing the RDF for a liquid at two temperatures, demonstrating how the peaks of the curves give the locations of the two shells surrounding the origin [13].

Intermediate Scattering Function

The ISF is a time-dependent correlation function which provides information about the behaviour of liquids upon supercooling. It is defined by the following equation:

$$F = \frac{1}{N}\langle \delta\rho_k(t)\delta\rho_{-k}(0)\rangle \tag{30}$$

Where K is the scattering vector in x direction, x_i (t) is the x-coordinate of the position particle i at a certain time t and the angular brackets indicate an ensemble average [3]. Note that it is not within the scope of this report to delve into its derivation.

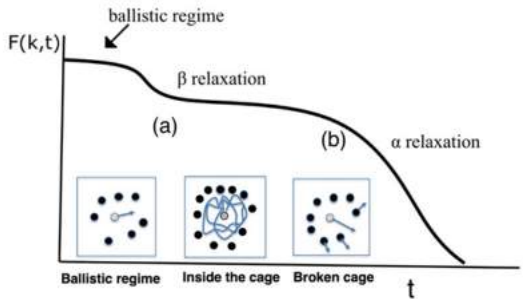

Figure 7: An example of an ISF plot, showing the three main regions to be found for a supercooled liquid [13].

In the context of this report, the ISF is used to characterise the relaxation times of a supercooled system. Figure 7 shows an example of an ISF plot. The initial decay is called the "ballistic" region, where particles diffuse without interaction with other particles. Two relaxation regions follow, the β-relaxation which appears as a plateau and crosses into the α-relaxation region. The β-relaxation refers to a period where particles "rattle in the cage" of the nearest neighbours; it lengthens in time the more supercooled a system is. The α-relaxation is reached when the particles finally "break out" of the cage and diffuse [13].

Mean Square Displacement:

The MSD measures the displacement of a particle from its origin, defined as:

$$< [\Delta r(t)]^2 >_N \tag{31}$$

where N is the number of "jumps" a particles has taken, and the sum of the individual "jumps" is

$$\Delta_r = \Delta_{r1} + \Delta r2 + ... + \Delta_{rn}(\Delta_{ri} = \pm a) \tag{32}$$

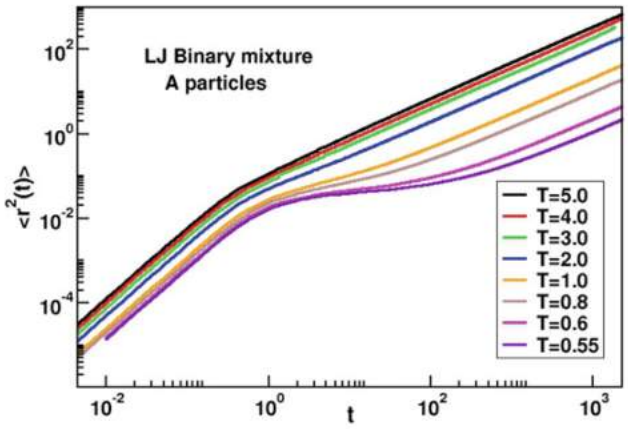

Figure 8: An MSD plot for a liquid at various temperatures, showing how a plateau emerges as the liquid is supercooled [13].

The MSD is always positive, and should increase as N increases. When plotted against time, the MSD for supercooled dynamics reflects an ISF plot, see Figure 8, showing an initial ballistics region, followed by a plateau where "rattling in the cage" occurs, eventually resulting in diffusion. As the MSD is proportional to time, its gradient can be used to calculate the diffusion coefficient, which is defined as:

$$D = \lim_{t\to\infty} 1/6d/dt[\Delta r_i(t))^2] \text{ [4]} \tag{33}$$

3 Methodology

3.1 Simulation Methods

Molecular dynamics computer simulations were run using Nvidia Geforce GTX 1080 graphics cards at Roskilde University (RUC) and the Roskilde University Molecular Dynamics (RUMD) package, version 3.6. Every simulation needed a python script to set parameters like the length of the simulation, temperature, density, and pair potentials. As well as a start file which contains the starting locations of the particles. The website rumd.org provides a tutorial that helps to get started with the start file and generate a starting configuration [2]. An example of the start file can be found in the Appendix.

The strategy was to learn to use RUMD and get a sense of MD simulations by starting with a KA three-component mixture provided by Prof. Thomas Schrøder at RUC. Then move on, to choose a different composition, followed by a different mixture. Simulations were run at a predefined density

and composition, KA 8:2:2 $\rho = 1.35$, at various temperatures to find a suitable temperature interval to work in (the composition indicates the ratio of particles, Type A:B:C). Temperatures that would not equilibrate within 50 million timesteps were considered too slow for this experiment. Between 15 and 25 state points was considered ideal per density per mixture to ensure enough data for the analysis.

Next, two more densities were decided upon, $\rho = 1.15$ and 1.2, and a further series of simulations was run. In the meantime, a new composition was chosen for the KA mixture, 8:2:4, and an appropriate density and temperature range to work in was found. The ratio 8:2:4 was chosen as we wanted to see how the mixture would behave with a markedly greater ratio of Type C particles.

A different model for a ternary mixture, WS 1:1:1, was then chosen based on several factors. Firstly, it was important to test a mixture with different masses. Secondly, it is an RS liquid, therefore, making excess entropy scaling more likely. As there is no reference point for a ternary WS mixture to be found, σ_{CC} was found by taking the mean of $\sigma_{AA}+\sigma_{BB}$. Similarly, $\sigma_{AC} = \sigma_{AA}+\sigma_{CC}$, and $\sigma_{BC} = \sigma_{BB} + \sigma_{CC}$. The same logic was used to find the mass of Type C, taken as the mean of m_A and m_B. An appropriate density and temperature range to work in was then found by trial and error.

The diffusion coefficient calculations were done in each case for particle A. Particle A means the major component except for the WS model where each particle has equal amounts. For the WS mixture, particle A is the largest particle. For every model, particle C means the third particle which was added to the already established binary mixture. RDF and MSD plots are shown in the results for different particle types. We ran out of time to discuss the universality of entropy scaling across different particle types.

3.2 Simulation Specifics

The KA mixture uses the LJ pair potential with the following parameters: $\sigma AA = 1.00, \sigma BB = 0.88, \sigma CC = 0.94, \sigma AB = 0.80, \sigma AC = 0.90, \sigma BC = 0.84; \epsilon AA = 1.00, \epsilon BB = 0.50, \epsilon CC = 0.75, \epsilon AB = 1.50, \epsilon AC = 1.25, \epsilon BC = 1.00$. Masses for particle types A, B and C are equal; $m = 1$. Cutoff is $rcut = 2.50\sigma$. For the KA 8:2:2 mixture, the densities used were $\rho = 1.2, 1.35, 1.50$, where the total number of particles $N = 12000$ and $T = 0.652 - 5.6$. For the 8:2:4 KA mixture, the densities used were $\rho = 1.15, 1.20$, where $N = 14000$ and $T = 0.5 - 5.2$. The time step range used was $0.002 - 0.005$. The length of the runs varied from $25600 - 839$ million timesteps, depending on state point.

The WS 1:1:1 mixture uses the same pair potential and rcut as the KA mixture, with the following parameters: $\sigma AA = 1.20, \sigma AB = 1.10, \sigma AC = 1.15, \sigma BB = 1.00, \sigma BC = 1.05, \sigma CC = 1.10; \epsilon AA = AB = AC = BB = BC = CC = 1$. Masses are $m_A = 2, m_B = 1, m_C = 1.5$. The densities used were $\rho = 0.5$ and 0.6, where the total number of particles $N = 900$ and $T = 0.5 - 6.0$. The timestep range used was $0.002 - 0.005$. The length of the runs varied from $25600 - 839$ million time steps, depending on state point.

3.3 Calculating the Diffusion Coefficient

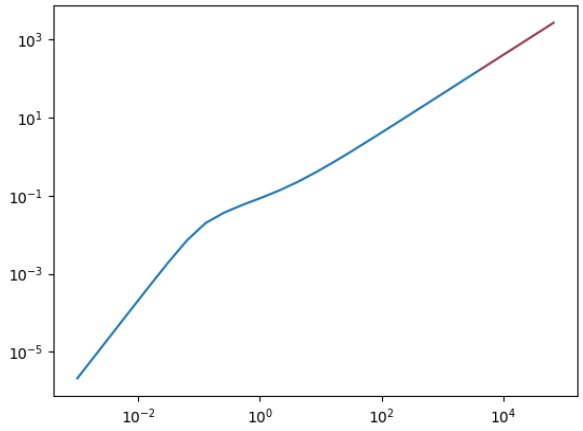

Figure 9: An example of how the slope of the MSD is taken. The red line is the best fit line for values in the later region of the MSD (blue line). The plot has been generated for each state point to check if the diffusion coefficient values can be used. (The presented plot is for KA 8:2:2, $\rho = 1.2$, $T = 0.7$.)

For each mixture, each state point is simulated for an appropriate number of time steps such that diffusion is reached, by checking the MSD plot and adjusting accordingly. The MSD file is then imported into a Python script which finds the slope of linear regression of the diffusion region of the MSD plot. Care is taken to make sure that an appropriate section of the diffusion region is considered in order to minimise statistical errors, see Figure 9. The gradient is then taken as a good approximation of the diffusion coefficient, recall Eq. 3 in Post-Processing [4].

The diffusion coefficient D is then converted to $\tilde{D}$; recall Eq. 3 in Section 2.1.2 [11].

3.4 Calculating the Excess Entropy

The excess entropy is calculated using a script written by Prof. Trond Ingebrigtsen [17] and adapted for ternary mixtures. The code can be found in the data set shared in Appendix A. The script is run using RUMD. It follows the calculations presented in Section 2.1.3. The file requires setting up the parameters of the model. The particle numbers and potentials between the particles have to be set. It needs a start file as well.

To start the calculations, first, a high enough temperature is set to be above the critical point then several small simulations are run where the virial Eq. 11 and potential energy Eq. 19 are calculated. Next, a Taylor polynomial is fitted to the virial values to get the virial function. Once the free energy is calculated for temperature at the set densities, then new simulations are started at constant density with varying temperatures. The potential energy is calculated for each temperature by summing up the potential energy for all particles. A polynomial is fitted to the potential energy values to get the potential energy function over temperature. This function is integrated which gives the free energy for the required temperatures. The excess entropy is calculated from the free energy and the potential energy (see Section 2.1.3).

An excess entropy calculation script is run for each density of each mixture; it gives the excess entropy values for all the temperatures set at that density.

The script outputs several files. First, the mean virial for each density is compared to the corresponding fitted virial. If the fitted virial curve gives a good approximation of the function of the virial for the system, the excess entropy values calculated by the script can then be used. The script also prints a file containing all the excess entropy values at a constant temperature, and changing densities. It is good for error-checking reasons but not necessary for finding the final results. Finally, the file containing excess entropy values for every temperature step is used to note the excess entropy values for the observed mixture.

4 Results

This section will firstly present a series of plots which give the reader a sense of the mixtures studied. The results for the individual mixtures, KA 8:2:2, KA 8:2:4 and WS 1:1:1 are then shown, followed by the results for the different compositions of the KA mixtures. Next, combined results for the WS and KA mixtures will be described and compared to the results for binary mixtures obtained in Ref.[6]. These results focus on majority particle Type A unless otherwise specified.

Note: As the terms mixture, model and system are interchangeable, "mixture" will be used to refer to KA or WS for the rest of the report in order to avoid confusion.

4.1 Post-Processing

Post-processing of the simulations was handled before the diffusion coefficient calculations and the excess entropy calculations. The purpose of this was two-fold; firstly, as a checkpoint during the experiment, and secondly, to give a sense of the type of mixtures being simulated. The following section presents relevant plots from each mixture; in order, mean-squared displacement, intermediate scattering function, the radial distribution function, the virial-potential plot. 3D visualisations of the mixtures generated by Open Visualisation Tool (OVITO) are also shown.

Mean Squared Displacement

The MSD plot for each mixture was checked in order to ensure that diffusion had been reached. All systems were run until the MSD reached $t = 10^1$, more than sufficient for a reliable diffusion coefficient calculation. Figures 10a, 10b and 11 show the MSD for the KA 8:2:2, KA 8:2:4 and WS 1:1:1 mixtures respectively, each for a given density and range of temperatures. The plots demonstrate the temperature dependence of the MSD; the lower the temperature, the slower the system reaches diffusion.

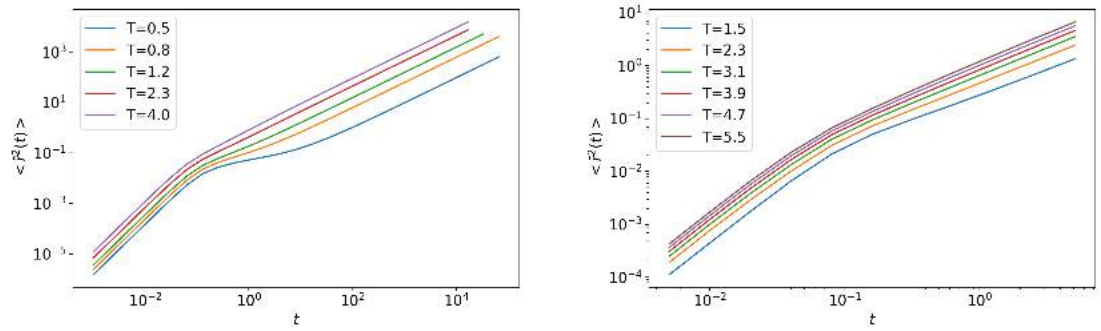

(a) (b)

Figure 10: (a) MSD for KA 8:2:2 mixture at $\rho = 1.2$ for five temperatures $T = 0.5, T = 0.8, T = 1.2, T = 2.3, T = 4.0$. (b) MSD for KA 8:2:4 mixture at $\rho = 1.2$ at six temperatures $T = 1.5, T = 2.3, T = 3.1, T = 3.9, T = 4.7, T = 5.5$.

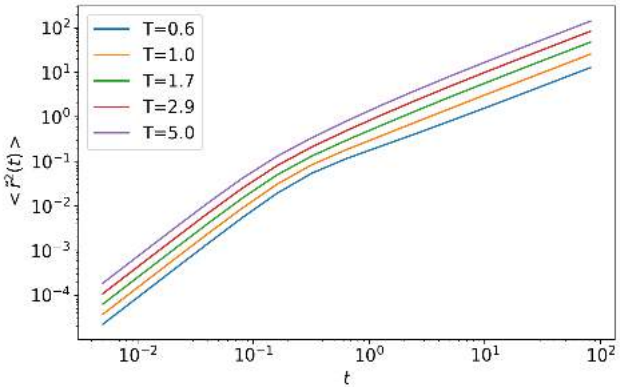

Figure 11: MSD for WS 1:1:1 mixture at $\rho = 0.6$ at five temperatures $T = 0.6, T = 1.0, T = 1.7, T = 2.9, T = 5.0$.

For KA 8:2:2 $\rho = 1.2$, in Figure 10a, when $T \geq 0.8$, it is clear that the system transitions quickly from the ballistics region to diffusion. At $T = 0.5$, a plateau is visible at $t \approx 10^1$, indicating that the particles are "trapped in the cage" between the ballistic and diffusion regions [13]. In contrast, KA 8:2:4 $\rho = 1.2$ in Figure 10b does not develop a plateau at the lowest temperatures; it is possible that this mixture does not descend far enough into supercooled territory. The mixture transitions straight from the ballistics region to the diffusion region at $t \approx 10^1$. Figure 11 shows the temperature dependence of the MSD for WS 1:1:1 $\rho = 0.6$, transitioning from ballistics to diffusion at $t \approx 10^{-.5}$, suggesting that it is the slowest mixture to relax of the three.

Figure 12a, 12b and 13 show the different MSD curves for particle types A, B and C, for KA 8:2:2 $\rho = 1.2, T = 0.5$, KA 8:2:4 $\rho = 1.2, T = 0.5$ and WS 1:1:1 $\rho = 0.6, T = 2.5$ respectively. Both Figures 12a and 12b show that the MSD for the three particle types are similar in the ballistic region, then differ in gradient in the diffusion region. KA pair potentials for AB, BB and BC are $\sigma = 0.80, 0.88, 0.84$ respectively, whilst pair potentials AA, AC and CC, have $\sigma = 1.00, 0.90, 0.94$. The lower σ values for pairs with Type B could explain the faster diffusion rates.

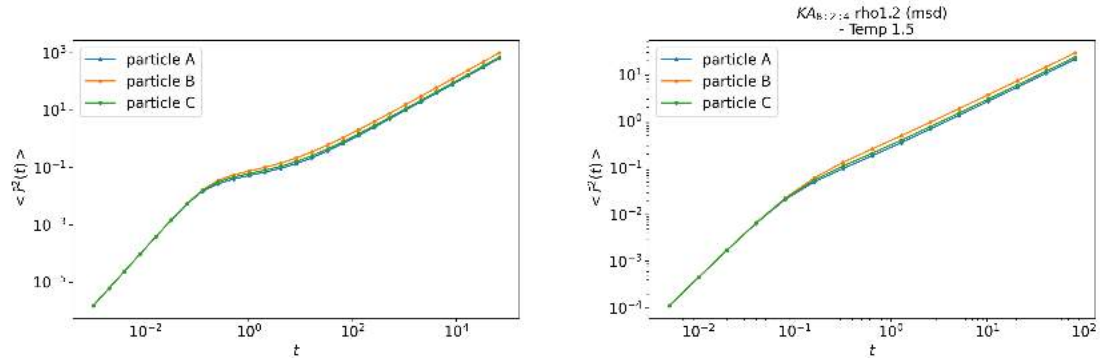

(a) (b)

Figure 12: (a) MSD for KA 8:2:2 mixture, $\rho = 1.2$ at $T = 0.5$ for all three types of particles (A,B and C). (b) MSD for KA 8:2:4 mixture, $\rho = 1.2$ at $T = 1.5$ for particle types A,B and C.

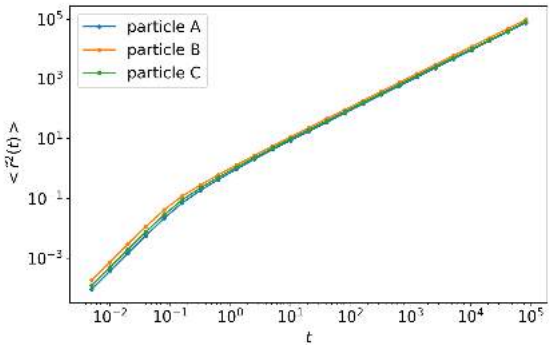

Figure 13: MSD for WS 1:1:1 mixture, $\rho = 0.6$ at $T = 1.0$ for particle types A, B and C.

Figure13, on the other hand, shows that the MSD for the three particle types differ in the ballistic region, then show a similar gradient in the diffusion region. This difference of gradients in the ballistic region could be due to the difference in masses of the particle types; Type B has the smallest mass and has the highest gradient of the three particles types.

All three figures demonstrate that all particle types reach diffusion before the diffusion coefficient values are calculated; this check was performed on all mixtures to reduce the risk of errors.

Intermediate Scattering Function

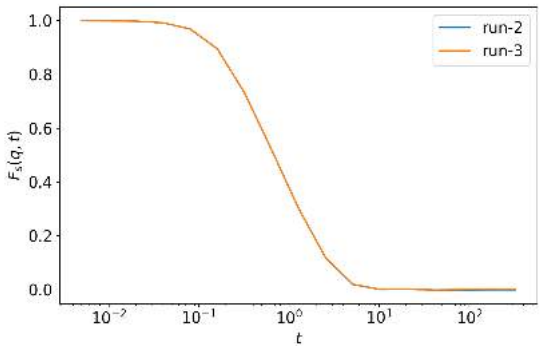

Figure 14: ISF for the WS 1:1:1 mixture with a density of $\rho = 0.6$ and temperature $T = 1.0$, how consecutive runs overlap when equilibrium is reached.

The ISF was used to check if each system had reached equilibrium. This was done by comparing the ISF plots of two consecutive runs; if the curves overlapped completely, then it was reasonable to consider the system had equilibrated, see Figure 14.

Figure 15a, 15b and 16 show the temperature dependence of the ISF for KA 8:2:2 $\rho = 1.2$, KA 8:2:4 $\rho = 1.2$ and WS 1:1:1 $\rho = 0.6$ respectively; it is clear that the relaxation time of the system lengthens as the temperature is lowered. For KA 8:2:2 $\rho = 1.2$, a plateau indicating β-relaxation has developed at $T = 0.5$, indicating that the system is approaching the glass transition. This plot reflects the plateau shown Figure 10a. Similar to their corresponding MSD plots, Figures 15b and 16 show that KA 8:2:4 $\rho = 1.2$ and WS 1:1:1 $\rho = 0.6$ transition straight from the ballistic region into α-relaxation. Again, this is possibly due to state points not being supercooled enough.

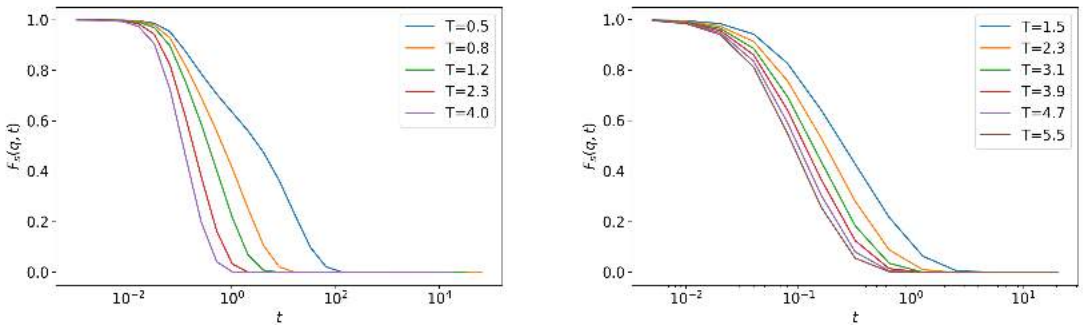

(a) (b)

Figure 15: (a) ISF for KA 8:2:2 $\rho = 1.2$ for five temperatures, $T = 0.5, T = 0.8, T = 1.2, T = 2.3, T = 4.0$. (b) ISF for KA 8:2:4 $\rho = 1.2$ for six temperatures, $T = 1.5; T = 2.3, T = 3.1, T = 3.9, T = 4.7, T = 5.5$.

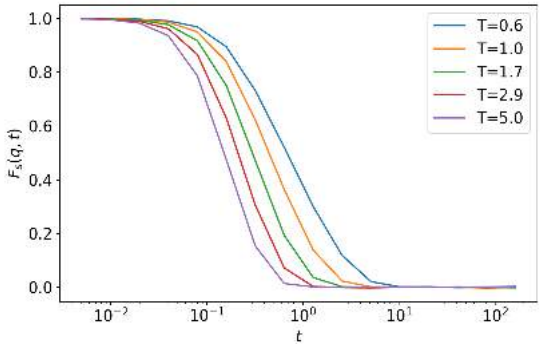

Figure 16: ISF for WS 1:1:1 $\rho = 0.6$ for five temperatures, $T = 0.6; T = 1.0, T = 1.7, T = 2.9, T = 5.0$.

Radial Distribution Function

The RDF was examined to ensure that each system was in a liquid state, see Figures 17, 18 and 19. All three figures demonstrate a change in $g(r)$ as temperature increases. The peak of the "first shell" of the RDF clearly decreases as temperatures increase for all three mixtures. Figure 17 and Figure 18 show that the second shell for the KA mixtures is at $r \approx 2$; this indicates that composition does not greatly affect the distance of the second shell. Figure 19 shows that the second shell for WA 1:1:1 $\rho = 0.6$ occurs at $r \approx 2.5$, this is most likely due to the pair potentials differing from the KA mixtures. In addition, Figure 19, shows the most statistical noise of the three mixtures; this could be due to the lower particle number in the mixture compared to the others. All three figures demonstrate that these ternary mixtures are liquids; this check was performed on all state points to reduce the risk of errors.

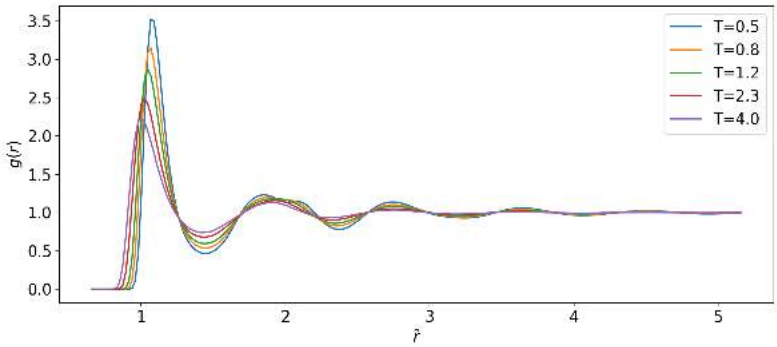

Figure 17: RDF for the KA 8:2:2 mixture at $\rho = 1.2$ for five temperatures, $T = 0.5, T = 0.8, T = 1.2, T = 2.3, T = 4.0$.

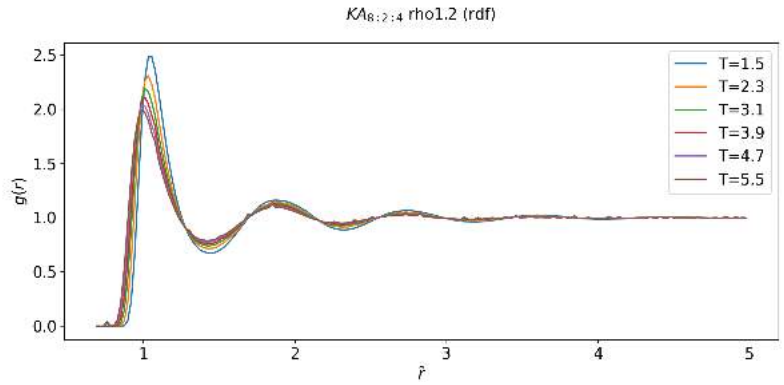

Figure 18: RDF for the KA 8:2:4 mixture at $\rho = 1.2$ for six temperatures, $T = 1.5, T = 2.3, T = 3.1, T = 3.9, T = 4.7, T = 5.5$.

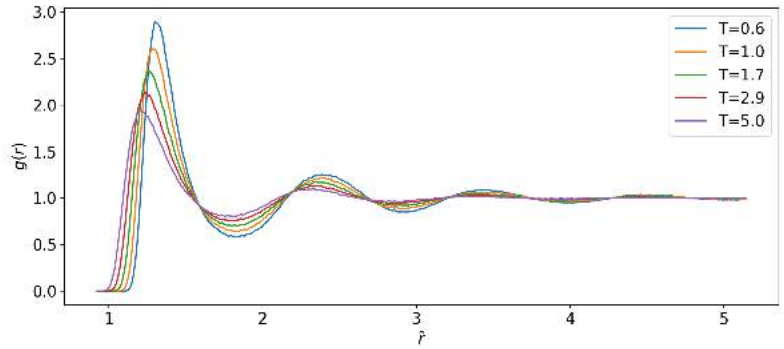

Figure 19: RDF for the WS 1:1:1 mixture at $\rho = 0.6$ for five different temperatures, $T = 0.6, T = 1.0, T = 1.7, T = 2.9, T = 5.0$.

Figures 20 and 21 display the RDF for all six combinations of particle pairs for KA 8:2:2 $\rho = 1.2$ at $T = 0.5$ and KA 8:2:4 $\rho = 1.2$ at $T = 1.5$ respectively. The figures show that pairs which include a Type A particle (AA, AB, AC) have the largest peaks in the first shell. This is most likely due to the majority particle, Type A, in all three combinations which increases the $g(r)$ value. In addition, the pairs BC and CC have larger $g(r)$ values in Figure 21 compared to Figure 20, most likely due to the higher ratio of Type C particles in KA 8:2:4.

Figure 22, where the RDF for all six combinations of particle pairs are shown for WS 1:1:1 $\rho = 0.6$ at $T = 0.6$, varies greatly in structure to the RDF for KA mixtures. Combinations AB and CC overlap perfectly, most likely due to their identical ϵ and σ values. The five curves are similar in shape, with first and second shells occurring in close proximity. This is possibly due to the mixture being composed of equal parts of each type of particle, giving only slight shifts in $g(r)$ values for all combinations. It is not clear how the different particle type masses affect the RDF.

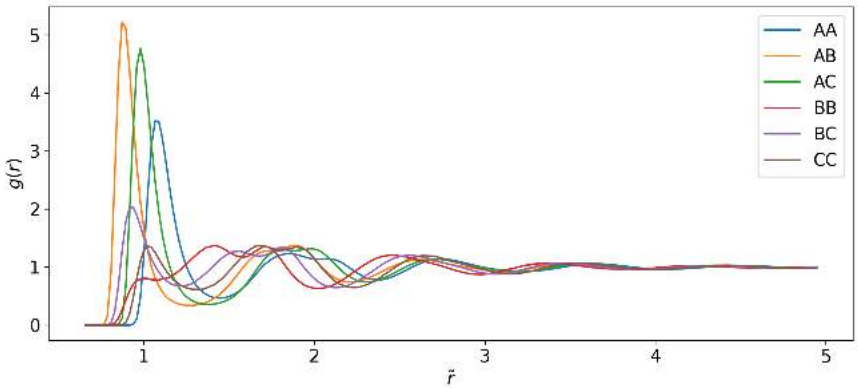

Figure 20: RDF for KA 8:2:2 $\rho = 1.2$, $T = 0.5$ for six particle combinations, AA, AB, AC, BB, BC, CC.

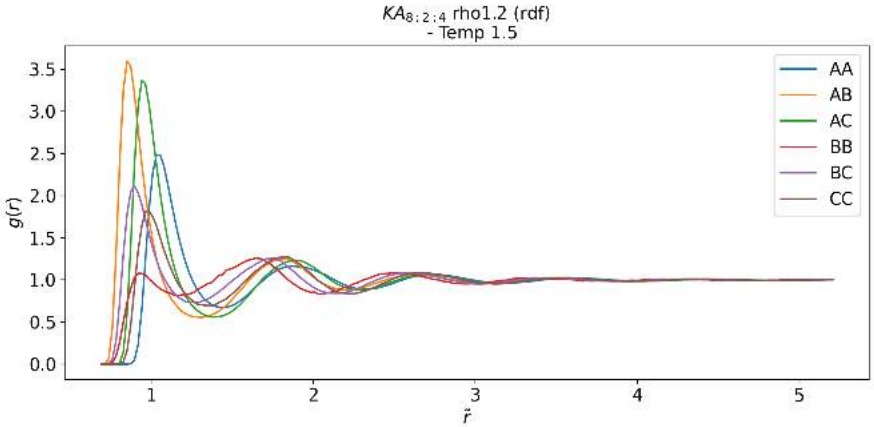

Figure 21: RDF for KA 8:2:4 $\rho = 1.2$, $T = 1.5$ for particle combinations AA, AB, AC, BB, BC, CC.

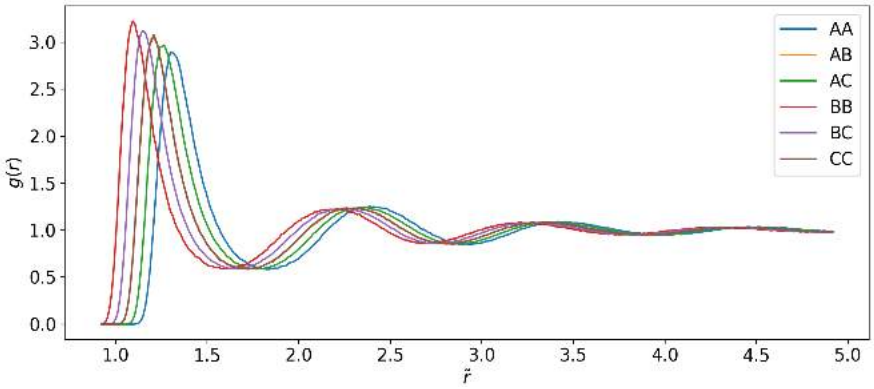

Figure 22: RDF for WS 1:1:1 $\rho = 0.6$, $T = 1.0$ for particle combinations AA, AB, AC, BB, BC, CC.

3D Visualisations

The OVITO visualisations for the systems were an extra check to make sure no crystallisation had occurred. Figures 23, 24, and 25 show the start configuration on the left and the end configuration on the right, for three different systems. Figure 23 is a representation of KA 8:2:2 $\rho = 1.5$ at $T = 3.2$, where Type A is orange, Type B is light blue and Type C is red. It is clear that the start configuration is not a crystal; it is already mixed and melted. The end configuration looks similar, with no discernible crystal structure. Figure 24 displays KA 8:2:4 $\rho = 1.2$ at $T = 2.3$, where Type A is lilac, Type B is green and Type C is yellow. The start configuration is in a crystal structure, while in the end configuration the particles are out of the lattice. Again, there are no noticeable crystal pockets visible. A similar observation can be made for Figure 25. It shows WS 1:1:1 $\rho = 0.6$ at $T = 1.0$, where Type A is green, Type B is pink and Type C is blue. As N = 900 for this system, it is easier to see the change in structure between start and end configurations; the crystal structure has completely melted.

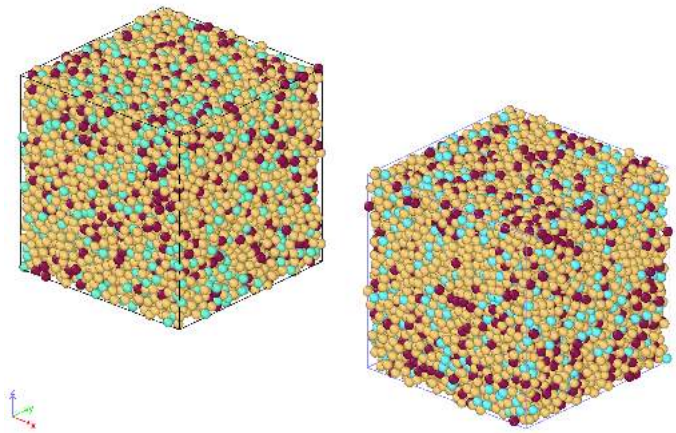

Figure 23: Visualisation of the simulation box for KA 8:2:2 $\rho = 1.35$, $T = 2.3$, showing the start configuration of the particles on the left, and the end configuration of the particles on the right.

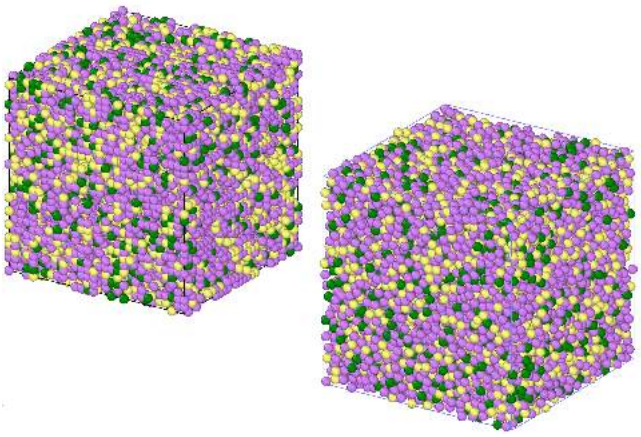

Figure 24: KA 8:2:4 mixture $\rho = 1.2$, $T = 2.3$ starts in a crystal lattice on the left. The end configuration on the right shows that that there is no crystallisation present.

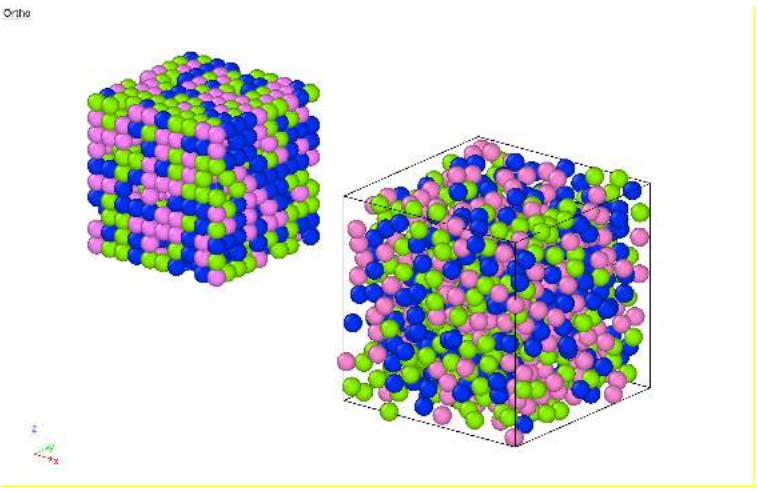

Figure 25: Visualisation of start and end configurations for WS 1:1:1 $\rho = 0.6$, $T = 1.0$, left and right respectively.

Virial-Potential Relationship

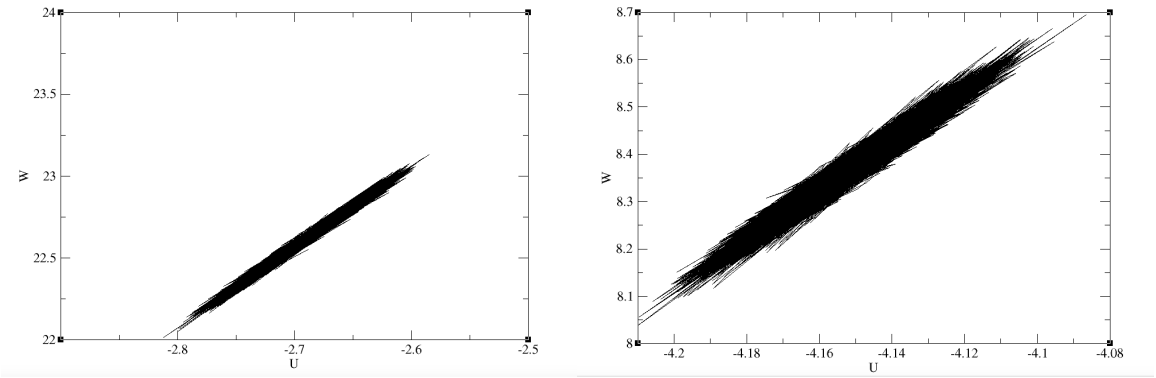

(a) (b)

Figure 26: (a) Scatterplot of the microscopic virial W vs. potential energy U for KA 8:2:2 $\rho = 1.35$, $T = 2.3$. This "blob" indicates that the liquid can be classified as an RS liquid. (b) Scatterplot showing virial W against potential energy U for KA 8:2:4 $\rho = 1.2$, $T = 1.5$.

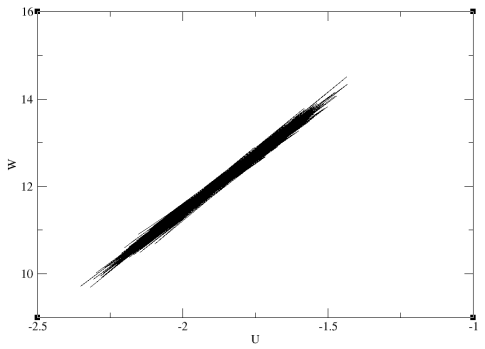

Figure 27: Scatterplot showing a strong correlation between the virial W and potential energy U for WS 1:1:1 $\rho = 0.6$, $T = 3.5$.

Recall that in Section 2.1.4 binary KA and binary WS mixtures are classified as RS liquids [18]. As ternary mixtures are not often studied, it was necessary to check if the ternary KA and ternary WS models are RS liquids as expected by plotting the microscopic virial W against the potential U. Figures 26a, 26b and 27 demonstrate that all three mixtures are RS liquids, as all three plots show a strong diagonal "blob", indicating the existence of thermodynamic isomorphs and preluding excess entropy scaling.

Diffusion Coefficient

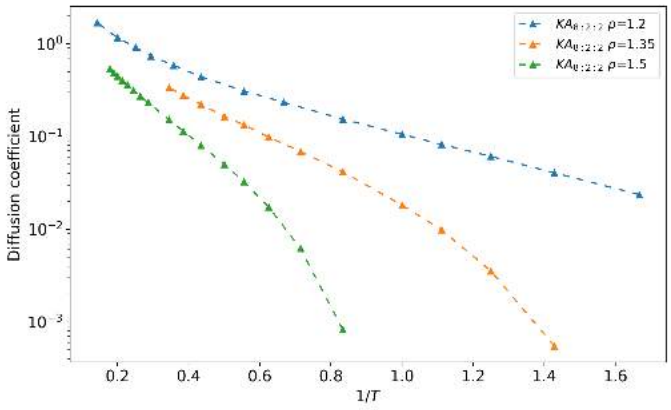

Figure 28: Diffusion coefficient vs. $1/T$ for the KA 8:2:2 mixture at various temperatures for three densities, $\rho = 1.2, \rho = 1.35, \rho = 1.5$. Each data point on the curves is the D value for a specific state point.

Figures 28, 29a and 29b display the diffusion coefficient D as a function of $1/T$ for KA 8:2:2, KA 8:2:4 and WS 1:1:1 mixtures respectively. Figure 28 shows the three densities studied for KA 8:2:2. An initial, linear decrease in D as $1/T$ increases can be seen for $\rho = 1.35$ and 1.5. $\rho = 1.35$ shows a deviation from the straight line in D around $1/T = 0.9$, whilst $\rho = 1.5$ shows an even steeper decrease in D around $1/T = 0.5$. This indicates a non-Arhennius function for these mixtures. In contrast, $\rho = 1.2$ displays a slight deviation in D from the straight line where $1/T \leq 0.4$; the curve seems to shift to a constant gradient around $1/T$ 0.4.

In Figure 29a, KA 8:2:4 $\rho = 1.2$ and 1.15 display a slight, non-linear decrease in D as $1/T$ increases; considering the scale of the plot, it could be said that the gradients are quite similar.

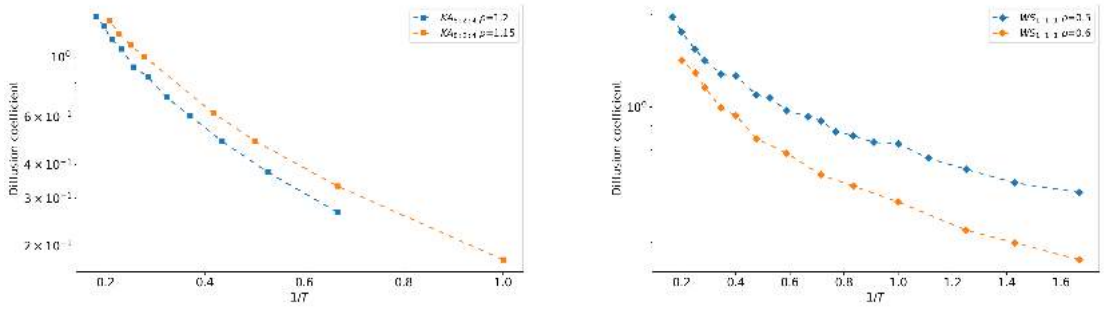

(a) (b)

Figure 29: (a) Diffusion coefficient as a function of temperature for the KA 8:2:4 mixture at various temperatures, for both $\rho = 1.2$ and $\rho = 1.15$. (b) Diffusion coefficient vs. $1/T$, for the WS 1:1:1 mixture at various temperatures, for $\rho = 0.5 and \rho = 0.6$.

Figure 29b shows two curves corresponding to two densities studied in WS 1:1:1, $\rho = 0.5$ and 0.6. Neither curve is smooth, with small deviations. However, a general sense of the shape of the curves is clear; both display an initial faster, non-linear decrease in D as $1/T$ increases. It should be noted that Figure 29b is on a different scale to Figure 28, therefore the deviations displayed here are not as large as they appear.

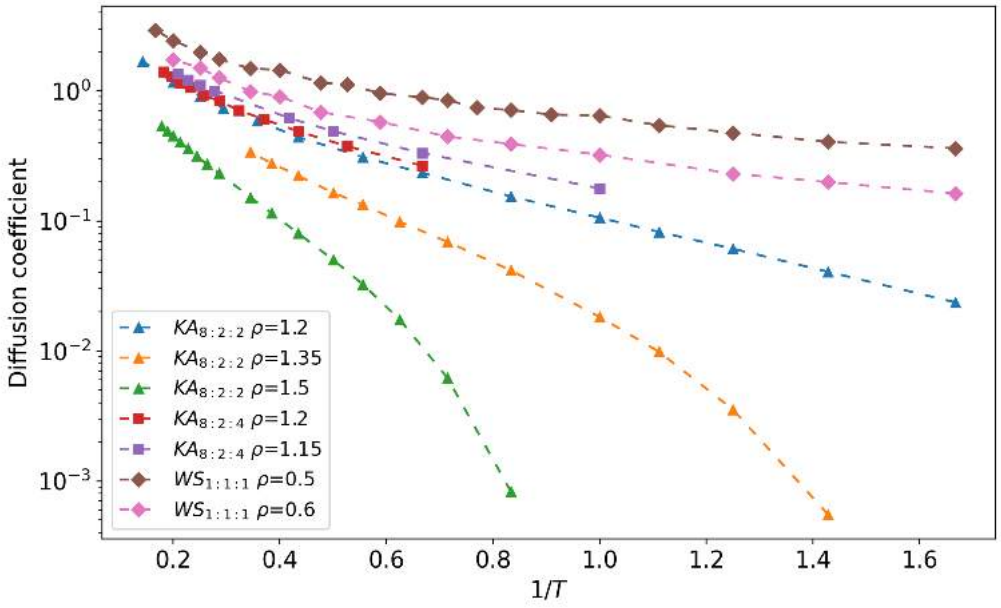

Figure 30: Diffusion coefficient against $1/T$, for the KA 8:2:2 mixture at $\rho = 1.2, \rho = 1.35, \rho = 1.5$ and various temperatures, the KA 8:2:4 mixture at $\rho = 1.2, \rho = 1.15$ and various temperatures, and the WS 1:1:1 mixture at $\rho = 0.5, \rho = 0.6$) and various temperatures.

Figure 30 displays the temperature dependence of the diffusion coefficient for all seven mixtures. Here, is it clear that WS 1:1:1 $\rho = 0.5$ and 0.6 are comparable to KA 8:2:2 $\rho = 1.2$ and KA 8:2:4

$\rho = 1.2$ and 1.15. The five curves have a similar initial accelerated decrease in D, then a shift to a constant decrease around $1/T \geq 0.4$.

4.2 Excess Entropy Scaling for Various Densities and Temperatures

Figures 31, 32 and 33 demonstrate that excess entropy scaling holds for the reduced diffusion coefficient $\tilde{D}$ for the KA 8:2:2, KA 8:2:4 and WS 1:1:1 mixtures, for up to three densities and several temperatures. In other words, there is an observed relationship between $\tilde{D}$ and S_{ex}, for various densities and temperatures. Figure 31 shows that $\rho = 1.2, 1.35$ and 1.5 for the KA 8:2:2 mixture collapse onto a universal curve to a good approximation. The curves clearly overlap where $-3.5 \leq S_{ex}/k_BN \geq -4.7$; where $S_{ex}/k_BN \geq -3.5$ there is not enough data for KA 8:2:2 $\rho = 1.35$ and 1.5 to show that the universality extends. Similarly, for $S_{ex}/k_BN \leq -4.9$, there is not sufficient data for KA 8:2:2 $\rho = 1.2$ to show that the universality continues. It is important to note that the curves for the lower densities appear to deviate in a non-trivial manner from KA 8:2:2 $\rho = 1.5$ as S_{ex}/k_BN decreases.

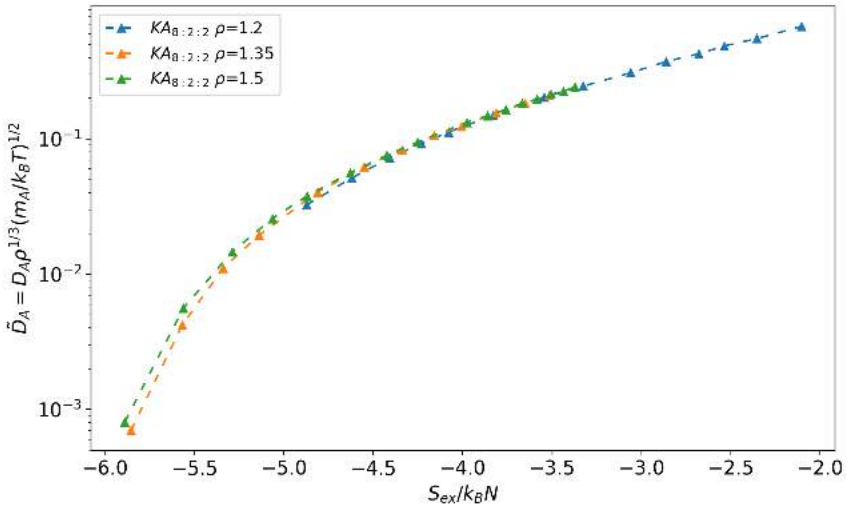

Figure 31: Excess entropy scaling for the diffusion coefficient of KA 8:2:2 for three densities, $\rho = 1.2, \rho = 1.35 and \rho = 1.5$. Each data point is a specific state point. An approximate collapse of the curves is seen.

There are two approximately straight lines corresponding to the two densities for KA 8:2:4 in Figure 32; the lines approximately overlap, indicating a quasi-universality of excess entropy scaling for the two densities. $\rho = 1.2$ shows slight deviations in $\tilde{D}$ for state points for $S_{ex}/k_BN \geq -2.7$.

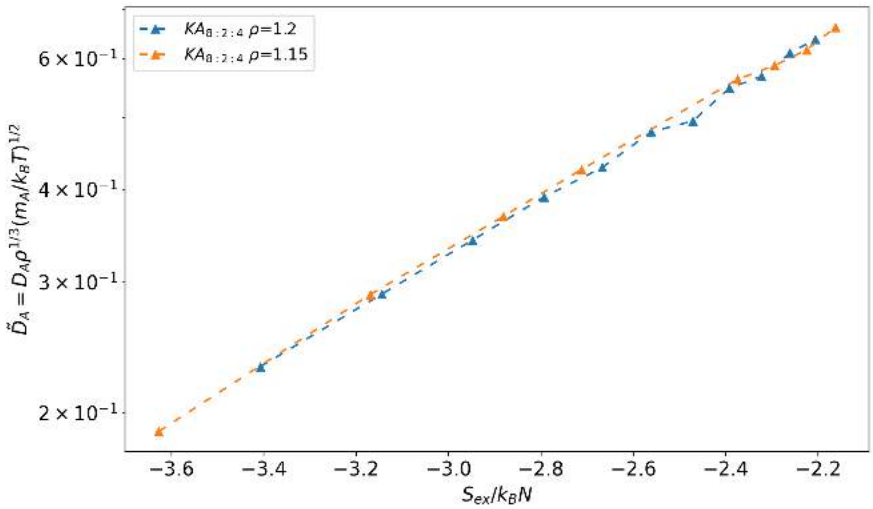

Figure 32: Excess entropy scaling for the diffusion coefficient of KA 8:2:4 for two densities, $\rho = 1.2$ and $\rho = 1.15$.

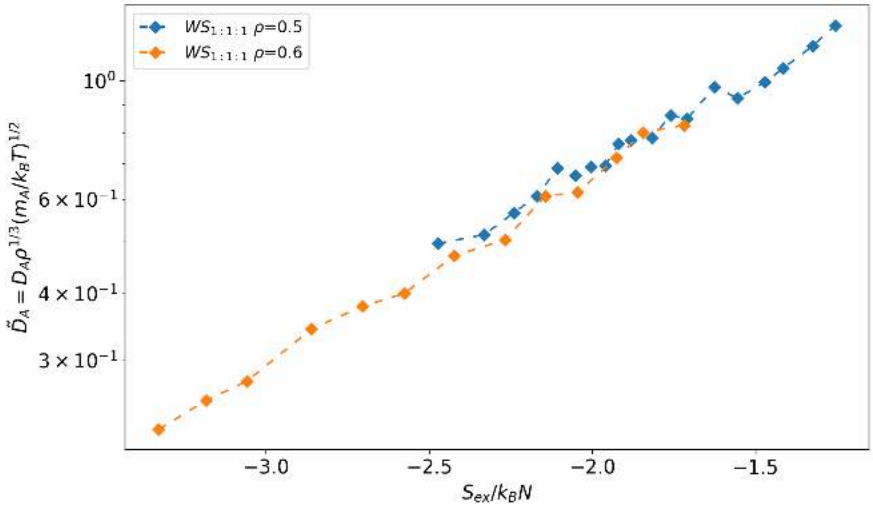

Figure 33: Excess entropy scaling for the diffusion coefficient of WS 1:1:1 for two densities, $\rho = 0.5$ and $\rho = 0.6$.

Figure 33 shows two curves, one for each density for WS 1:1:1; the curves have some deviations, however, a linear path can be approximated for both $\rho = 0.5$ and $\rho = 0.6$. Outside of $-2.5 \geq S_{ex}/k_B N \leq -1.7$, the curves do not overlap; $\rho = 0.5$ extends beyond $S_{ex}/k_B N \geq -1.7$, and $\rho = 0.6$ extends beyond $S_{ex}/k_B N \leq -2.5$. This discrepancy could be explained by elevated statistical noise for this mixture due to the lower number of particles in the system ($N = 900$) compared to the KA mixtures ($N = 12000 - 14000$). Considering the scale of the plot, quasi-universality is is observed despite the slight deviations between the curves.

4.3 Excess Entropy Scaling as a Function of Composition

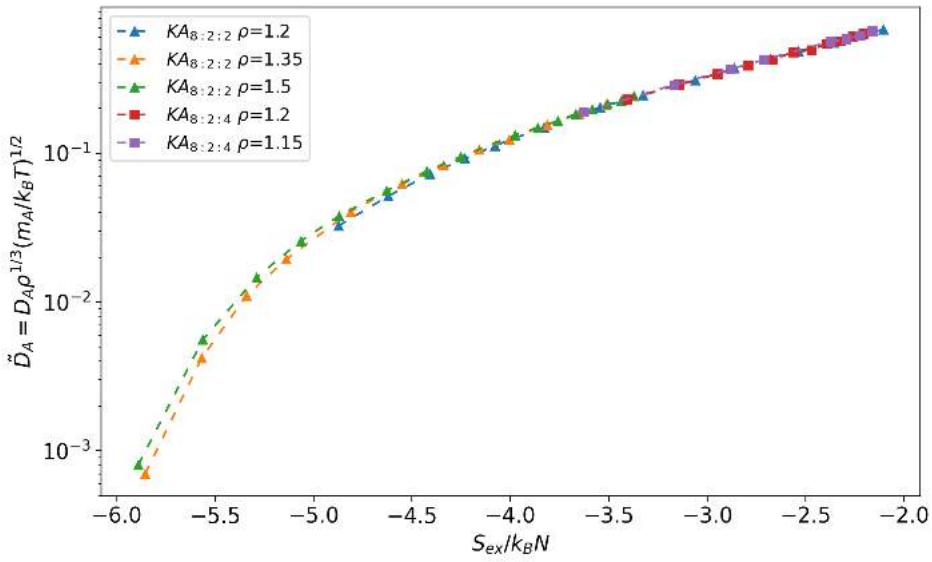

Figure 34: Excess entropy scaling for the diffusion coefficient of KA 8:2:2 at various temperatures for three densities ($\rho = 1.2, \rho = 1.35, \rho = 1.5$), as well as KA 8:2:4 at various temperatures for two densities ($\rho = 1.2, \rho = 1.15$). An approximate collapse of the plots is shown.

Now that excess entropy scaling has been demonstrated for fixed compositions of ternary mixtures, it is necessary to show that it continues to hold if composition is treated as a variable, in addition to density and temperature. Figure 34 shows that $\tilde{D}$ as a function of $S_{ex}/k_B N$ for various densities and temperatures of KA 8:2:2 and KA 8:2:4 collapse onto a quasi-universal curve. It should be noted that the curves for KA 8:2:4 are shorter than the curves for KA 8:2:2, however they clearly overlap KA 8:2:2 $\rho = 1.2$ in the region $-3.2 \geq S_{ex}/k_B N \leq -2.1$.

4.4 Excess Entropy Scaling Between Ternary Mixtures

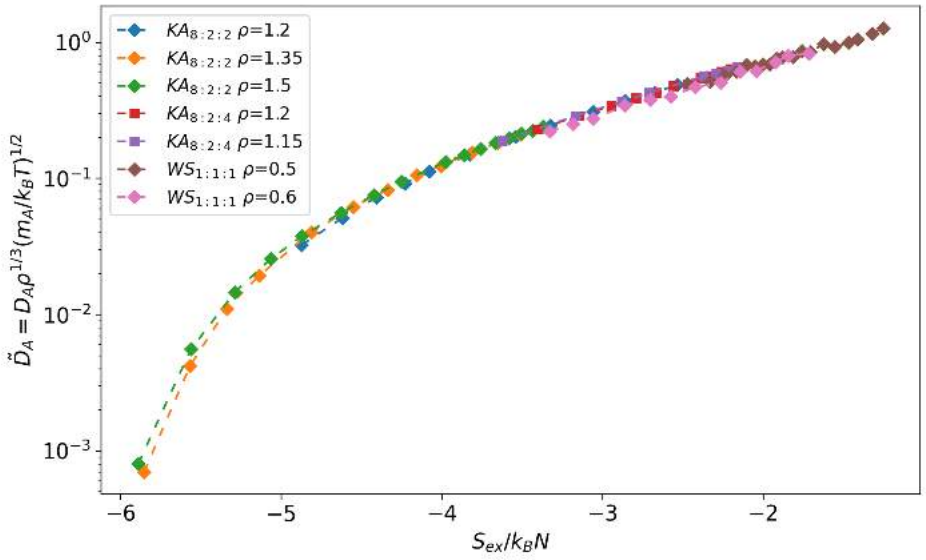

Figure 35: A comparison of the diffusion coefficient as a function of excess entropy for all mixtures studied. Shown, KA 8:2:2 at various temperatures for three different densities ($\rho = 1.2, \rho = 1.35, \rho = 1.5$), KA 8:2:4 at various temperatures for two densities ($\rho = 1.2, \rho = 1.15$) and WS 1:1:1 at various temperatures for two densities ($\rho = 0.5$, $\rho = 0.6$). An approximate collapse of all the curves can be observed.

As a logical next step, excess entropy scaling for all the ternary KA and WS mixtures are compared, to see if the relationship continues to hold, see Figure 35. It appears that all seven curves collapse to a good approximation barring the deviations in the lower S_{ex} region, thus a quasi-universal relationship is observed. It could be stated that excess entropy scaling appears to hold between ternary mixtures. Specifically, the KA 8:2:4 and WS 1:1:1 curves overlap in the same region of the plot; KA 8:2:2 $\rho = 1.2$ is the only KA 8:2:2 curve which overlaps with the KA 8:2:4 and WS 1:1:1 curves. It should be noted that the slight deviations in the WS 1:1:1 curves seen in Figure 33 are also visible here on this scale, to a lesser extent.

4.5 Excess entropy scaling Amongst Binary and Ternary Mixtures

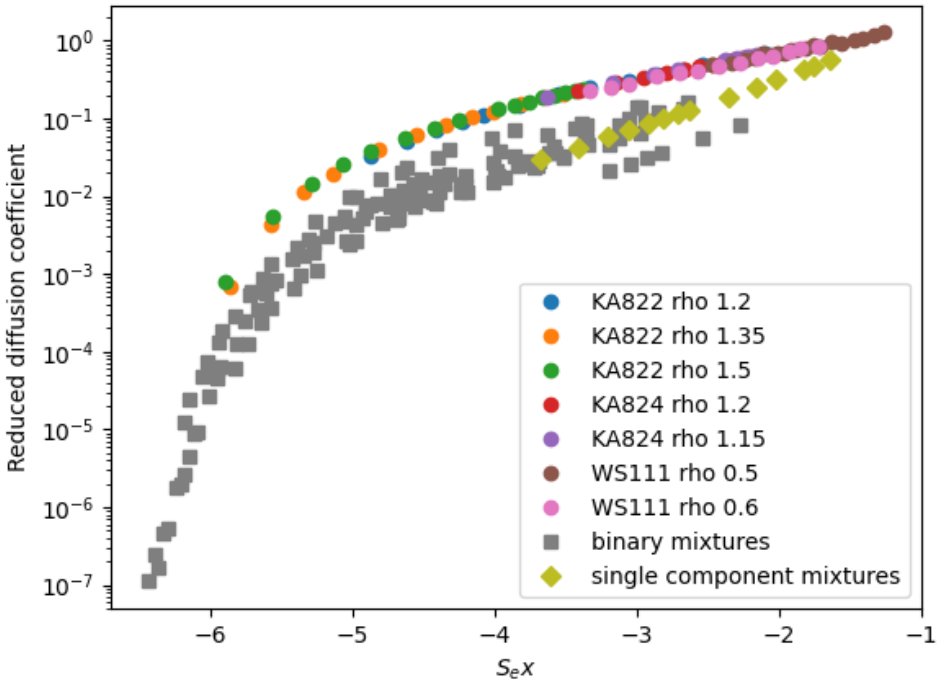

Figure 36: Excess entropy scaling for the diffusion coefficient for the various ternary mixtures studied in this experiment (colourful circles), compared to the binary mixtures studied in ref. [6] (grey squares), with a SCLJ model as reference (green diamonds).

Finally, the excess entropy scaling found amongst binary mixtures in "Excess-Entropy Scaling in Supercooled Binary Mixtures" [6] is compared to the results amongst ternary mixtures from this report with a SCLJ model as reference, see Figure 36. Here, a clear collapse is not seen between the ternary mixtures and the binary mixtures, although it appears that the ternary mixtures follows a similar path to the quasi-universal curve for binary mixtures. The ternary curve has higher $\tilde{D}$ values and does not intersect the binary curve at any point, however this could be due to a lack of data in the lower S_{ex} region.

5 Discussion

When we look at the diffusion coefficient D plotted against temperature T in Figure 30, for any mixture with a fixed density ρ changes in temperature define a curve. This is expected, given that D is a function of T and ρ. What is unexpected, however, is that a correlation is seen when the reduced diffusion coefficient $\tilde{D}$ is plotted against excess entropy S_{ex}, as shown in Figures 31, 32, 33. For any given mixture at a given density, a curve is defined. The question is, do these curves collapse for different densities and temperatures, different compositions, and different ternary mixtures? And finally, how does the excess entropy scaling of ternary mixtures relate to that observed recently in binary mixtures?

5.1 To what extent does excess entropy scaling hold for various densities and temperatures?

KA 8:2:2

The densities, $\rho = 1.2, 1.35$ and 1.5, studied for the KA 8:2:2 mixture collapse onto a quasi-universal curve when the diffusion coefficient is plotted against excess entropy, Figure 31. The collapse appears precise especially for excess entropy values greater than -4.0. For lower excess entropy values, the curves for $\rho = 1.35$ and 1.5 diverge slightly. It is unclear if this divergence is a result of possible experimental errors or if it is a characteristic of the excess entropy scaling of ternary mixtures.

It is important to point out that in Figure 28, it can be seen that KA 8:2:2 $\rho = 1.35$ and $\rho = 1.5$ appear to be increasingly supercooled, which would render the diffusion coefficient increasingly sensitive to changes in temperature. In this particular supercooled region, slight errors in excess entropy calculations could appear more drastic. This suggests that more precise calculations are required. Additionally, more simulations are needed to further observe this phenomenon, for example by simulating lower temperatures for $\rho = 1.2$.

KA 8:2:4

In Figure 29a, the KA 8:2:4 mixtures have not yet reached the supercooled region. However, the limited available data for this composition (see Figure 32) closely line up to define a quasi-universal curve, suggesting that excess entropy scaling applies to this mixture.

WS 1:1:1

The simulations of the WS 1:1:1 mixture do not reach deeply supercooled states either, as visible in Figure 29b. It would have been ideal to model lower temperatures and higher densities for more applicable data with regards to excess entropy scaling. In addition, small irregularities can be observed in the results, likely a result of experimental errors, for example time steps which were too large for such "high" temperatures. One should perhaps consider our collective inexperience in MD simulations as a factor which could have affected the precision and range of the results. That being said, Figure 33 clearly gives an approximate collapse, indicating that the correlation holds.

5.2 To what extent is there quasi-universality as a function of composition?

In order to see if excess entropy scaling continues to hold across compositions, the two compositions of the KA mixture are compared; namely, KA 8:2:2 to KA 8:2:4. The small amount of data available for the KA 8:2:4 mixture limits the discussion here. Based on the results displayed in Figure 34, quasi-universality of excess entropy scaling holds across different compositions. The state points of the KA 8:2:4 mixtures overlap with the curve for $\rho = 1.2$ of the KA 8:2:2 mixture. It should be reiterated that all the excess entropy scaling plots show the reduced diffusion coefficient for particle Type A, which is the majority component in both compositions KA 8:2:2 and KA 8:2:4. Increasing the ratio of particle Type C in the KA mixture does not appear to significantly influence excess entropy scaling in this case.

5.3 To what extent is there quasi-universality as a between ternary models?

Figure 35 displays all mixture curves in one plot, showing that all the state points collapse to a quasi-universal curve for ternary mixtures studied. This result is not entirely unexpected, given that all the mixtures simulated are RS liquids. However, it is neither an entirely expected result given the inexperience of the team and the novel three-component mixtures used in the experiments. As the excess entropy scaling of ternary supercooled mixtures is an ongoing research area without major findings and publications to date, more research is required to see if quasi-universality continues to hold further into supercooled regions, as well as across more ternary mixtures, including non-RS liquids.

5.4 To what extent does quasi-universality hold amongst binary and ternary models?

Upon comparing the excess entropy scaling of ternary mixtures to binary mixtures, Figure 36 shows that the quasi-universal curve defined by ternary mixtures is similar in form to the quasi-universal curve of binary mixtures. However, for the same excess entropy values, the ternary mixtures have higher diffusion coefficients than the binary mixtures and single-component model. In addition, it appears that the ternary mixtures have a more precise collapse than the binary mixtures, which poses the question, does the third component provide stability to excess entropy scaling? It would have been ideal to simulate four and five component models and observe how the correlation evolved. Unfortunately, time limitations prevented this ambition from being fulfilled during the course of this project.

5.5 Experimental Procedure

Some considerations should be given to the possible flaws in experimental procedure due to lack of experience in MD simulations. Knowledge had to be built from the ground up with regards to excess entropy scaling and computer simulations, after which came the challenge of getting to know the RUMD program used and how to best set up a MD experiment. A prior working knowledge of these techniques would have allowed us to avoid unnecessary mistakes during the experiment. Therefore, some aspects of the results may reflect this amateur approach.

Statistical Noise

The KA mixtures were simulated with greater than 10000 particles, while the WA 1:1:1 mixtures were simulated with 900 particles. This large difference in simulation size is reflected in the RDF plots; there is more statistical noise observed in Figure 19 compared to Figures 17 and 21. It is unknown to what extent this noise, caused by poor statistics due to a smaller simulation size, affects the results. As an attempt to mitigate the noise, WS 1:1:1 simulations were run for a greater number of time steps in order to ensure that the simulations were well into the diffusion region, as seen in Figure 11, before the diffusion coefficient D was calculated. Time allowing, larger simulations for WS 1:1:1 would have been ideal, so as to ascertain if statistical noise can be reduced by increasing particle numbers, or if it is due to some other issue with the experiment.

Excess Entropy Calculation Errors

The precision of excess entropy S_{ex} calculation depends on two main parameters. Firstly, it depends on how good the fit of the microscopic virial W and potential energy U is; this was checked for each mixture, and no major irregularity occurs between the values given by the simulations and

the fit. Secondly, the starting point of the integration of W over density ρ should be chosen such that the ρ value is low enough to bring the entropy value of the mixture as close as possible to that of an ideal gas. Several excess entropy calculation scripts were run to get an understanding of how the starting point of the integration changes the results. Lowering the starting value of ρ gave a more precise collapse for curves of different mixtures, suggesting that S_{ex} calculations were improved by this technique. Several other S_{ex} calculation scripts were run to test the effects of changing starting temperature, lengths of simulation time steps, and frequency of simulations (for temperatures and densities).

6 Conclusion

To reiterate the research question, how does excess entropy control transport properties in supercooled ternary mixtures? Despite minor deviations, the results indicate quasi-universal excess entropy scaling across different temperatures for a given mixture, a collapse which continues to hold across the two compositions of the KA mixture, KA 8:2:2 and KA 8:2:4; as well as across two different models, the KA model and the WS model. This quasi-universality appears to operate in a similar, but not equivalent manner to the correlation found for binary mixtures in Ref. [6]. Figure 36 shows that the reduced diffusion coefficient $\tilde{D}$ values for ternary mixtures are consistently higher for any given excess entropy S_{eX} value than for binary mixtures. Additionally, these preliminary results show a more precise collapse for ternary mixtures compared to binary mixtures. These observations suggest that the effect of an additional component could be significant and raises the question if this deviation continues as the number of components is increased in supercooled mixtures.

The general theme of this conclusion is that even though the results are promising, the subject is clearly in need of more data. Future work could include simulating KA and WA mixtures at lower temperatures, exploring more KA and WA compositions, finding more three, four, five-component models to simulate, in order to examine if excess entropy scaling continues to hold. It would seem a necessary step to check both RS and non-RS multi-component liquids, as well as compare excess entropy to other transport coefficients. Furthermore, the experimental procedure could be tweaked with experience, optimising parameters for excess entropy calculation and overall noise reduction.

This report has been an immense learning experience both theory-wise and in a hands-on manner; given the opportunity, we would be interested in exploring this area of research further. For example, a clear route of investigation from our ending point would be to ascertain how particle types in ternary models affect excess entropy scaling. Beyond the obvious skills gained during the course of this semester, perhaps the most important learning outcome has been a deeper understanding of how physicists apply theory. Which leaves us with a question which continues to intrigue, are transport properties are a function of excess entropy, or vice versa?

A Simulation Files

Simulation result files and sample run files can be found via the following link:
https://doi.org/10.5281/zenodo.7650090

References

[1] Leapfrog integrator, July 2020. URL `https://www.johndcook.com/blog/2020/07/13/leapfrog-integrator/`. Accessed on 20. Dec. 2022.

[2] Rumd tutorial, Jan 2021. URL `http://rumd.org/doc-3.6/index.html`. Accessed on 20. Dec. 2022.

[3] B. Ackerson, P. Pusey, and R. Tough. Interpretation of the intermediate scattering function at short times. *The Journal of Chemical Physics*, 76(3):1279–1282, 1982.

[4] M. P. Allen and D. J. Tildesley. *Computer simulation of liquids*. Oxford university press, 2017. ISBN 978–0–19–880320–1.

[5] I. H. Bell. Probing the link between residual entropy and viscosity of molecular fluids and model potentials. *Proceedings of the National Academy of Sciences*, 116(10):4070–4079, 2019.

[6] I. H. Bell, J. C. Dyre, and T. S. Ingebrigtsen. Excess-entropy scaling in supercooled binary mixtures. *Nature communications*, 11(1):1–12, 2020.

[7] A. Cavagna. Supercooled liquids for pedestrians. *Physics Reports*, 476(4-6):51–124, 2009.

[8] J. C. Dyre. Colloquium: The glass transition and elastic models of glass-forming liquids. *Reviews of modern physics*, 78(3):953, 2006.

[9] J. C. Dyre. Roskilde simple liquids' quasiuniversality. *DNFR Center "Glass and Time"*, 2013.

[10] J. C. Dyre. Hidden scale invariance in condensed matter. *The Journal of Physical Chemistry B*, 118(34):10007–10024, 2014.

[11] J. C. Dyre. Perspective: Excess-entropy scaling. *The Journal of chemical physics*, 149(21): 210901, 2018.

[12] L. S. Ettre. Nomenclature for chromatography (iupac recommendations 1993). *Pure and Applied Chemistry*, 65(4):819–872, 1993.

[13] P. Gallo and M. Rovere. *Physics of Liquid Matter*. Springer, 2021.

[14] S. A. Hollingsworth and R. O. Dror. Molecular dynamics simulation for all. *Neuron*, 99(6): 1129–1143, 2018.

[15] N. Hoze and D. Holcman. Statistical methods for large ensemble of super-resolution stochastic single particle trajectories. *bioRxiv*, page 227090, 2017.

[16] G. I. Periodic boundary diagram. URL `https://en.wikipedia.org/wiki/Periodic_boundary_conditions`. Accessed on 20. Dec. 2022.

[17] T. S. Ingebrigtsen. Rumd scripts for free-energy calculations of atomic mixtures, rigid molecules, and atomic solids. URL `https://github.com/tsingebrigtsen/FreeEnergyCalculation`. Accessed on 20. Dec. 2022.

[18] T. S. Ingebrigtsen. *From isomorphs in molecular liquids and confinement to molecular dynamics at constant potential energy*. PhD thesis, Danish National Research Foundation Centre" Glass and Time", 2013.

[19] A. D. Parmar, M. Ozawa, and L. Berthier. Ultrastable metallic glasses in silico. *Physical Review Letters*, 125(8):085505, 2020.

[20] M. E. Rosen, C. P. Grant, and J. Dallon. Mean square displacement for a discrete centroid model of cell motion. *Plos one*, 16(12):e0261021, 2021.

[21] Y. Rosenfeld. Relation between the transport coefficients and the internal entropy of simple systems. *Physical Review A*, 15(6):2545, 1977.

[22] S. Toxvaerd, U. R. Pedersen, T. B. Schrøder, and J. C. Dyre. Stability of supercooled binary liquid mixtures. *The Journal of chemical physics*, 130(22):224501, 2009.

[23] G. Wahnström. Molecular-dynamics study of a supercooled two-component lennard-jones system. *Physical Review A*, 44(6):3752, 1991.